Mapping and Quantifying Plasma Fibronectin Matrices in Whole Body Homeostasis

Mir Hamed Nabavi

Faculty of Dental Medicine and Oral Health Sciences

McGill University, Montreal, Canada

February 2023

A thesis submitted to the Faculty of Graduate Studies and Research in partial fulfillment of the requirements of the degree of M.Sc. in Dental Science.

Table of Contents

ABSTRACT

Fibronectins (FN) are a family of multifunctional, extracellular matrix (ECM) glycoproteins that are known to play important roles in fundamental processes related to adhesive and migratory behavior of cells, including embryogenesis, cancer development, wound healing, and maintenance tissue integrity. There are two types of FN: cellular FN (cFN) and plasma FN (pFN). pFN is produced by hepatocytes in liver and secreted into circulation as a soluble, globular form at concentration of ~300-600 µg/ml both in humans and mice. pFN can accumulate from blood into tissues where it assembles an insoluble form in ECM. Altered levels of pFN have been seen in a variety of illnesses, such as cancer, different stages of liver disease, diabetes, coronary heart disease, and periodontal disease. In these pathological conditions, low or high pFN levels may be associated with the disease status and act as a disease modifier and a biomarker. pFN distribution in specific organs and tissues throughout in the whole body is not completely assessed. The aim of this study is to establish a method that allows for the quantification and qualitative assessment of the distribution of a fluorescence-labeled pFN in different organs and tissues of the body. For this method, pFN was labeled with AlexaFluor-568 and AlexaFluor-680 injected intraperitoneally to C57bl/6 mice (male, 12 wk age) every day in three consecutive days. Mice were euthanized, tissue dissected and used to either protein extraction followed by quantitative fluorometry (for AlexaFluor-568 labeled material) or histological fixation and fluorescence microscopy (for AlexaFluor-680 labeled material to circumvent autofluorescence at lower wavelengths). Metabolic tissues were used as a pilot project. Two histological approaches were tested: paraffin embedding/sectioning and cryogenic preparation/sectioning. Fluoroimaging confirmed that injected pFN located from peritoneal space to serum and remained intact as a protein. Fluorometric quantification of AlexaFluor-568-pFN showed its abundant presence in visceral adipose tissue (AT), subcutaneous AT, serum, liver, bone marrow, and pancreas. Comparing the two histological approaches, cryosectioning appeared superior, but yet fluorescence signal was not optimal and requires further improvement. According to our findings, fluorometry is a highly suitable way for measuring pFN matrix formation in different tissues. This study identified AT as tissues where pFN forms ECM and where it may have a novel role in regulating AT function.

RÉSUMÉ

Les fibronectines (FN) sont une famille de glycoprotéines multifonctionnelles de la matrice extracellulaire (ECM) qui sont connues pour jouer un rôle important dans les processus fondamentaux liés au comportement adhésif et migratoire des cellules, comme l'embryogenèse, le développement du cancer, la cicatrisation des plaies et le maintien de l'intégrité des tissus. Il existe deux types de FN : la FN cellulaire (cFN) et la FN plasmatique (pFN). La pFN est produite par les hépatocytes dans le foie et secrétée dans la circulation soluble forme globulaire à une concentration d'environ 300-600 μg/ml chez l'homme et la souris. La pFN peut s'accumuler dans le sang dans les tissus où elle assemble une insoluble dans l'ECM. Des niveaux altérés de pFN ont été observés dans diverses maladies, telles que le cancer, les différents stades de la maladie du foie, le diabète, les maladies coronariennes et les maladies parodontales. Dans ces conditions pathologiques, un niveau de pFN faible ou élevé peut être associé à l'état de la maladie et agir comme un modificateur de la maladie et un biomarqueur. La distribution de la pFN dans des organes et des tissus spécifiques dans tout le corps n'est pas complètement déterminée. Le but de cette étude est d'établir une méthode qui permet la quantification et l'évaluation qualitative de la distribution d'unepFN marqué par fluorescence dans différents organes et tissus du corps. Pour cette méthode, la pFN a été marqué avec AlexaFluor-568 et AlexaFluor-680 et injectée par voie intrapéritonéale à des souris C57bl/6 (mâles, âgés de 12 semaines) chaque jour pendant trois jours consécutifs. Les souris ont été euthanasiées, les tissus disséqués et utilisées pour l'extraction des protéines suivie d'une fluorométrie quantitative (pour le matériel marqué AlexaFluor-568) et pour fixation histologique et microscopie de fluorescence (pour le matériel marqué AlexaFluor-680 pour contourner l'autofluorescence à des longueurs d'onde plus petites). Les tissus métaboliques ont été utilisés comme projet pilote. Deux approches histologiques ont été testées : l'inclusion/la section en paraffine et la préparation et la section cryogénique. La fluoroimagerie a confirmé que la pFN injectée se situait dans l'espace péritonéal et dans le sérum et restait intact en tant que protéine. La quantification fluorométrique d'AlexaFluor-568-pFN a montré sa présence abondante dans l'AT viscérale, l'AT sous-cutanée, le sérum, le foie, la moelle osseuse et le pancréas. En

comparant les deux approches histologiques, la section cryo est apparue supérieure, mais toutefois, le signal de fluorescence n'était pas optimal et nécessite par la suite une amélioration. Selon nos découvertes, la fluorométrie est une technique très appropriée pour mesurer la formation de la matrice pFN dans différents tissus. Cette étude a identifié AT comme des tissus où pFN forme l'ECM et où il peut avoir un nouveau rôle dans la régulation de la fonction AT.

ACKNOWLEDGMENTS

First and foremost, I would like to express my deepest and most sincere gratitude to my supervisor, Dr. Mari Kaartinen, for accepting me in her lab and for her guidance over the duration of my degree. She has been an immensely supportive and encouraging mentor. I am forever grateful to her for believing in me and giving me the opportunity to learn under her mentorship and the constant guidance in every step of my experiments.

I would also like to express my deepest gratitude to the Ph.D. students in our lab (Sahar Ebrahimi Samani, Fatemeh Soltani, Mahdokht Mahmoodi, and Elahe Mirzarazi Dahaghi). They taught me various laboratory techniques so patiently and allowing me to learn from their vast experience.

Outside of our immediate lab, I would like to give special thanks to my thesis committee members, Dr. Murshed, and Dr. Reinhardt, for taking the time to attend my annual progress meeting and provide me with insightful feedback and recommendations for my project. I appreciated Dr. Murshed showing me how to use a fluorometer in his lab. I thank Dr. Reinhardt for allowing me to use the microscope in his lab and Neha Dinesh for training me on the microscope and fluorescent imaging. I also thank Valentin Dan Nelea, for his invaluable help with the French translations of my abstract. I thank Dr. Moffatt for providing a fluoroimager and Matthew Tiranardi for helping me in reading samples with the fluoroimager.

Lastly, I would like to thank my core support group: my mother, my father, and my brothers, who all provided me with unwavering support from the beginning till the end.

CONTRIBUTION OF AUTHORS

Mir Hamed Nabavi: *Faculty of Dental Medicine and Oral Health Sciences, McGill University, Montreal, Canada*: wrote the text in the thesis, generated figures in the thesis, and did the major experiments (labeling procedures-determining degree of labeling- cell and tissue IF staining-Injection- mice dissection-protein extraction-analyzing and interpreting data-Frozen embedding of specimens -protein measurements- reading and gathering fluorometer data- capturing IF images)

Mari T. Kaartinen: *Associate Professor, Faculty of Dental Medicine and Oral Health Sciences, McGill University, Montreal, Canada*: Supervised and designed the whole study and edited the text and figures in this thesis.

Mahdokht Mahmoodi: *Faculty of Dental Medicine and Oral Health Sciences, McGill University, Montreal, Canada:* gave 3T3-L1 cells.

Elahe Mirzarazi-Dahagi: *Department of Anatomy and Cell Biology, Faculty of Medicine and Health Sciences, McGill University, Montreal, Canada*: aided in the preparation of gel for fluoroimaging.

Histology Core, Goodman Cancer Research Center McGill University: did paraffin embedding and sectioning of specimens.

LIST OF FIGURES

Figures 1,3 and 17 are created with BioRender.com

LIST OF ABBREVIATIONS

FN	Fibronectin
ECM	Extracellular Matrix
pFN	Plasma Fibronectin
cFN	Cellular Fibronectin
AF	Alexa Fluor
AT	Adipose Tissue
VAT	Visceral Adipose Tissue
SAT	Subcutaneous Adipose Tissue
BAT	Brown Adipose Tissue
Wk	Week

1 INTRODUCTION

1.1 Liver

1.1.1 Liver anatomy and function

The liver is the largest organ in the body, accounting for approximately 2 % of the whole body or about 1.5 kilograms (3.3 pounds) in the average adult human. The functional unit of the liver is the liver lobule. The human liver contains 50,000 to 100,000 individual lobules. The liver lobule is located around a central vein and is composed of many liver cellular plates. The thickness of each liver cellular plate is two layers of cells. Between these two cell layers are bile canaliculi, which drain into bile ducts in the fibrous septa, dividing the neighboring liver lobules [1].The liver has two lobes, and it is located in the right upper quadrant of the abdominal cavity under the right hemidiaphragm. It is protected by the rib cage and kept in place by ligamentous attachments [2].

The liver can restore itself after significant hepatic tissue loss from either partial hepatectomy or acute liver injury. In partial hepatectomy, up to 70 percent of the liver is removed, but the remaining lobes widen and restore the liver to its original size. This rapid regeneration requires only 5 to 7 days in rats. During liver regeneration, hepatocytes replicate once or twice. After the liver's original size and volume are achieved, hepatocyte proliferation returns to its normal level [1].

1.1.2. Protein metabolism of liver

Loss of liver's function and contribution to protein metabolism causes death in a few days. The most critical functions of the liver in protein metabolism are the following:

- Deamination of amino acids
- Formation of urea for removal of ammonia from the body fluids
- Formation of plasma proteins
- Interconversions of the various amino acids and synthesis of other compounds from amino acids [1]

Deamination of amino acids is needed when they are used for energy or converted into carbohydrates or fats. The liver is the main organ for Deamination in the body. The deamination process forms large amounts of ammonia. If the liver does not assemble urea, the plasma ammonia concentration rises rapidly, resulting in hepatic coma and death.

The liver can assemble plasma proteins at a maximum rate of 15 to 50 g/day. Thus, even if half the plasma proteins are lost from the body, they can be refilled in 1 or 2 weeks. Plasma protein shortage drives rapid mitosis of the hepatic cells and growth of the liver to a larger size, resulting in rapid production of plasma proteins until the plasma concentration returns to normal [1].

Among the liver's most important functions are its ability to synthesize certain amino acids and interconversion of them to other essential biochemical compounds [1].

1.1.3. Hepatokines

Hepatokines are proteins secreted by hepatocytes, and they can affect many mechanisms in the body through autocrine, paracrine, and endocrine signaling [3]. Quantitative analysis displayed that the mouse liver proteome and plasma proteome contain 7,099 and 4,727 proteins, respectively. A total of 1818 proteins are common in the liver and plasma (25.6% of the liver proteins and 38.5% of the plasma proteins are common). This overlap implies that up to ~25% of liver proteins are potentially secreted into the circulation [4]. Some of the important hepatokines are listed below: albumin, C-reactive protein, and FN; proteins that regulate hemostasis and fibrinolysis; carriers such as apolipoproteins; and proteins that regulate metabolism [3].

Albumin is the most abundant hepatocyte-derived protein in the human body. Albumin accounts for 55-60% of the plasma proteins. The total albumin in a 70 kg healthy adult is about 250-300g. The plasma compartment contains 42% of total albumin, and the rest is in the extravascular compartments. The skin, muscle, gut, and liver are significant locations of albumin in the extravascular pool. Each day, 120–145 g of albumin is lost into the extravascular space. Most of this is reabsorbed into circulation by lymphatic drainage. Only the liver can produce albumin in humans. Albumin is not stored by the liver, and it is released into the portal circulation as soon as it is produced. In healthy adults, the

synthesis rate is nearly 12–25 g of albumin per day. The colloid osmotic pressure of the interstitial fluid surrounding the hepatocyte is the most significant regulator of albumin production. Total daily albumin degradation in a 70 kg adult is around 14 g day−1. Albumin is degraded in many organs. Nearly half of the albumin is broken down in muscle and skin [5]. The albumin production rate depends on nutritional intake. Fasting declines albumin synthesis, and a no-protein-diet causes a more significant drop in albumin production [6]. Disease changes the distribution of albumin between the intravascular and extravascular parts. The altered distribution in acute disease is related to increased capillary leakage [7]. The albumin production rate may be changed in the diseases. Positive acute-phase proteins like C-reactive protein have higher gene transcription rates during the acute-phase response to injury, inflammation, or sepsis, whereas albumin transcription synthesis decreases [8].

1.2. Fibronectin

Fibronectin (FN), a 220 kDa glycoprotein, is secreted as a dimer (440 kDa) that is covalently bonded by two disulfide bonds located close to each protein's C terminus. It is a widely distributed protein that can be found in the blood, skin, lungs, and many other tissues [8].

1.2.1. Fibronectin structure

FN comprises two similar subunits of 220 to 250 kDa bound by disulfide bonds at the carboxyl-terminate, creating the characteristic FN dimer. Each FN monomer is formed by variable combinations of three homologous repeating parts termed Types Ⅰ, Ⅱ, and Ⅲ, that are connected by short peptide segments. There are twelve Type I, two Type Ⅱ, and fifteen to seventeen Type Ⅲ homologous repeats in each FN sequence. A single exon encodes Type Ⅰ and Type Ⅱ modules. In contrast, Type Ⅲ modules are coded for by 2 exons except for extra domains A and B and the ninth Type Ⅲ domain [9] (**Figure 1**). Remarkable molecular subunit diversity results from the complicated splicing of the FN primary transcript at three specific sites that code for the Type Ⅲ domains, EIIIA and EIIIB [8, 10].

The FN isoforms are divided into two main categories based on solubility and tissue source: the soluble plasma FN (pFN) and the insoluble cellular FN (cFN). pFN is exclusively produced by hepatocytes in the liver and secreted into the blood at concentrations of 0.3 mg/ml in humans and 0.6 mg/ml in mice [11, 12]. pFN always lacks the EDA and EDB domains. The V region is present in just one subunit of pFN dimer [13]. cFN is synthesized and deposited into the ECM by a variety of cell types, including fibroblasts, smooth muscle cells (SMCs), endothelial cells, and osteoblasts. Due to cell-specific and developmental-specific patterns of alternative splicing, which result in the presence of either EDA, EDB, or both, it consists of a broader and more heterogeneous group of FN isoforms. There are other variations in cFN that lack both domains [14, 15].

Some post-translational modifications of the FN molecule, such as phosphorylation and sulfation, have been observed. These modifications do not make significant differences among isoforms [16]. All forms of FN have considerable amounts of carbohydrates. The carbohydrate content of cFn variants is higher than that of pFn [8].

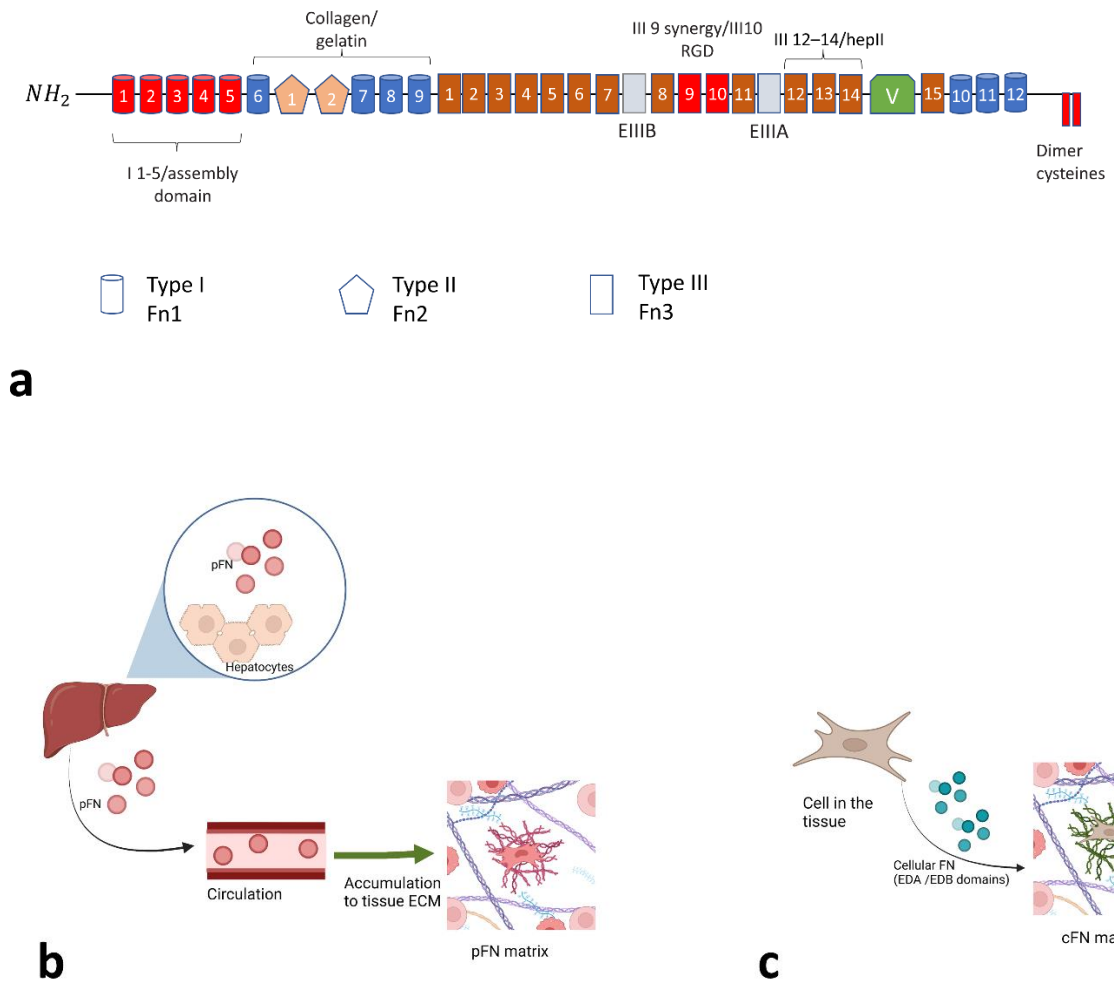

Figure 1. **Structure of FN**. (*a*) Each FN subunit has three different repeat types: Type I (cylinder), Type II (pentagon), and Type III (rectangle). The cell-binding domain (RGD site in III10 + synergy site in III9), the N-terminal assembly domain (I1–5), and the intermolecular dimer cysteines at the C terminus (red parts) are domains necessary to start matrix assembly. (*b*) Hepatocytes in the liver generate pFN, which then leaves the liver and enters the bloodstream to spread to many other tissues and form pFN matrixes. (*c*) cFN is generated and deposited into the ECM by tissue-resident cells and contains EDA /EDB domains.

1.2.2. Fibronectin functions

The complex structure of FN and its presence in almost all tissue and plasma suggest that this protein plays a significant role in fundamental biological processes. FN gene inactivation during early murine embryonic development is lethal [17]. The amino-terminal part of FN is formed by Type I homologous repeats that can bind to various substrates, including matrix heparin and cell-surface heparan sulfate proteoglycans, glycosphingolipids found in membranes of central nervous system tissues, and bacteria [8] (**Figure 1**). This domain also can covalently bind to fibrin, an insoluble plasma protein critical to blood clotting, via factor ⅩⅢa transglutaminase-catalyzed cross-linking [18]. The FN's highly glycosylated collagen/gelatin binding site is near the amino-terminal domain. The same domain that attaches to collagen can also attach to the C1q component of the complement system, which can facilitate FN's involvement in the clearance of immune complexes and cellular debris during the body's defense response. The carboxyl end of FN contains the molecule's primary heparin-binding region. It also contains Type Ⅲ repeats and a variable segment [8] (**Figure 1a**).

1.2.3. Fibronectin matrix assembly

FN is assembled into a fibrillar matrix in many tissues and throughout all stages of life and in normal and pathological situations. Homozygous FN gene inactivation results in early embryonic death and causes severe malformations in tissues descended from mesoderm; Notochord and somites are absent, and the heart and embryonic arteries are deformed. These embryonic abnormalities may result from fundamental deficits in mesodermal migration, adhesion, proliferation, or differentiation due to the absence of FN [17]. FN fibrils form meshworks networks around cells and connect neighboring cells (**Figure 1b**). EM images show that the diameter of FN fibers is 5-25 nm. Early fibroblast cultures predominately have thin fibrils; however, in a mature matrix, the fibrils thicken. FN has two subunits connected to each other by disulfide bonds at the C terminus of each subunit. Disulfide bonds play a critical role in the multimerization of dimers into fibrils[19]. FN is the ligand for the integrin family of adhesion receptors. Integrins on the cell surface bind the RGD (Arg-Gly-Asp) sequence in FN. FN Type III (FN III) includes multiple repeats of a 90-amino-acid, and FN III 10 has sites for cell attachment. The primary receptor for

FN matrix assembly is α5β1 integrin, which attaches to the RGD sequence in FNIII10 and the synergy site in FNIII9 [20, 21]. Anti-integrin or anti-FN antibodies block integrin-cell binding domain interactions and prevent fibril formation [22]. FN in a solution environment has a compact shape and cannot form fibrils even in high concentrations. Fibril formation in the blood can create life-treating effects [23].

1.2.3.1. Major steps in FN matrix assembly

An FN dimer attaches to two integrin receptors on cell surface, and the cytoplasmic domains of the integrins bind to intracellular proteins, and these intracellular proteins are also linked to the actin cytoskeleton. These attachments can increase cell contractility, apply forces that stretch FN and unravel its protein folding which change it from compact to linear form. FN binding induces integrin clustering, and these clusters in turn bring high concentrations of FN to the cell surface. A high concentration of FN is essential for FN-FN interactions because when FN shape changes from compact form to linear form, its cryptic binding sites are exposed which again promotes FN-FN interactions and self-assembly. One of the actin cytoskeleton functions is to facilitate interactions between integrins and FN. Deleting the β integrin cytoplasmic domain or depolymerization of actin with specific drugs prevents FN matrix assembly [19]. FN matrix assembly is a dynamic and ongoing process [24]. FN fibrils are separated when shear forces are applied to attached cells [25].

1.2.4. Fibronectin role in wound healing

FN matrices create the wound's initial ECM structure, which is replaced by collagen [26]. The collagen binds to the collagen binding sequence on FN (FNI6FNII1-2FNI7-9). This interaction between FN and collagen causes collagen deposition and assembly over FN matrices. This interaction is also beneficial for the FN matrix, and it can protect the FN matrix from microenvironmental forces [27].

Wound healing has four phases as below:

1- hemostasis, 2- inflammation, 3- proliferation, 4- remodeling

FN plays a role in all stages of wound healing. Plasma FN has a role in the initial stage of wound healing and clot formation [28] and assembling cell-ECM [29]. Cellular FN regulates the later stages of wound healing [29].

In the hemostasis phase, plasma FN assists the clot formation and helps platelet aggregation. Platelets increase plasma FN matrix assembly in the inflammation phase via an increase in platelet binding site expression. FN has opsonic properties and can help phagocytosis to clear foreign pathogens in the inflammation phase [30].

During the inflammatory response, proteolytic enzymes degrade FN to FN fragments, and FN fragments (particularly 110–120 kDa) prevent apoptosis of injured parenchymal cells [31]. FN is associated with collagen I during proliferation phase (granulation tissue). In this phase, temporary FN matrix is replaced by collagen type I matrix [28]. In the remodeling phase, turnover of the FN matrix is necessary; excessive FN matrix buildup in this stage causes scar tissue formation or fibrosis [32].

Von Willebrand factor (vWF) and fibrinogen are the essential ligands supporting platelet thrombus formation and thrombus growth. Mice lacking in fibrinogen showed no evident defect in thrombus growth, except in the stability of large thrombi, but mice deficient in β3 integrins cannot form a thrombus. FN content of platelets deficient in fibrinogen is much higher than WT platelets, suggesting that FN plays a critical role in thrombus formation in the absence of fibrinogen or even when fibrinogen is present [33]. In Heyu et al. study, pFN knockout was used to evaluate the impact of pFN on clot formation; the pFN and platelet FN levels decreased to 2 % and 20%, respectively, in pFN knockout mice. Then the mice were evaluated in terms of the clot formation speed. The pFN deficiency did not affect the initial platelet adhesion. However, compared to control mice, a delay of several minutes in thrombus formation was observed in the arterioles of pFN-deficient mice. The authors concluded that FN, Von Willebrand factor (vWF), and fibrinogen are essential factors in thrombus initiation, growth, and stability [33]. Matuskova et al. reported a delay in clot formation in FN heterozygous (FN-/+) mice. In these mice, the amount of pFN dropped to half the normal level. When pFN was injected into these mice, the clot formation rate returned to normal, which showed the incorporation of injected pFN into the developing thrombi [34].

Both pFN and cFN play a role in forming and organizing smooth muscle cells (SMCs), the major cell type in the vascular wall. FN is essential for the development of blood vessels before birth and blood vessel homeostasis from birth to adulthood. In the absence of cFN, pFN can be replaced in the aortic wall and act as a safeguard for vascular stability [35].

1.2.5. Liver diseases and plasma FN production

pFN is synthesized and secreted by hepatocytes. Tamkun et al. have shown that hepatocytes produce progressively more pFN with time in cell culture. The ratio of FN to albumin secretion is about 1:10 during days 3 to 5 in cell culture, but this ratio increases over time[11]. Additionally, it has been demonstrated that perfused rat liver can synthesize all of the pFN needed by the body in ten hours [36].

1.2.5.1. Liver fibrosis

Dysregulation in the normal healing process and scar formation can cause fibrosis. Liver fibrosis is caused by almost all chronic liver illnesses, including autoimmune and viral hepatitis, pharmacological side effects, iron buildup, alcohol intake, and biliary obstruction [37]. FN can regulate cell adhesion and proliferation; thus, it has a critical role in progression of fibrosis [38]. The predominant ECM component in fibrosis is collagen type I, whereas FN levels rise prior to collagen buildup [37]. FN expression is required for collagen matrix assembly. When FN assembly inhibitor is used on hepatic stellate cells, both FN and collagen levels in the ECM levels are decreased, and FN inhibitor can reduce fibrosis and collagen synthesis during liver fibrogenesis [39]. Furthermore, FN can modulate responsiveness of stellate cells to active transforming growth factor-β (TGF-β); in this way, FN can protect against excessive liver fibrogenesis [37]. Injection of carbon tetrachloride (CCl4) induces liver fibrosis in rats. In this rat model of liver fibrosis, expression of FN (FN), TGF-β, and α-smooth muscle actin (SMA) are increased after the injection, and their expression levels are returned to their baseline level when treatment with CCl4 is terminated. Therefore, FN expression increases in the beginning stage of liver fibrosis [37].

1.2.5.2. Serum fibronectin levels in acute and chronic viral hepatitis patients

Viral Hepatitis is caused by several well-known hepatotropic viruses including hepatitis A, B, C, and D. Also, other viruses such as the hepatitis G virus (HGV), transfusion-transmitted virus (TTV), TTV-like mini virus (TLMV), TTV variants (including SANBAN, TUS01, PMV, and YONBAN), SEN virus (SENV) subtypes (including SEN-V-D and SEN-V-H), Epstein-Barr Virus, cytomegalovirus, herpes simplex virus, varicella zoster virus, and rubella can cause hepatitis [40]. Acute self-limited hepatitis caused by the hepatitis A and E viruses is spread by blood; however, Hepatitis B, C, and D viruses are parenterally transmitted and lead to chronic hepatitis. In the chronic stage, the disease lasts more than six months [40].

In chronic hepatitis, the level of aspartate aminotransferase (AST) and alanine aminotransferase (ALT) in the blood goes up, but the level of albumin and bilirubin are usually normal in the serum [41]. The normal level of FN in human plasma is about 300 ± 100 µg/mL [42]. pFN levels decrease in both acute and chronic hepatitis, which is rooted in the fact that its production decrease and its consumption increases. In chronic hepatitis, pFN levels rise after interferon therapy. Furthermore, the degree of liver inflammation and pFN levels are inversely correlated [40, 43]. In addition, serum FN levels are negatively correlated with serum AST, ALT, and GGT levels. Since the levels of the enzymes AST, ALT, and GGT in the blood are higher in severe than moderate hepatitis, it has been suggested that serum FN levels might help determine the severity of hepatitis [40].

In western countries, drug use and alcohol abuse are the main reasons for liver failure, but in eastern countries, particularly China, hepatitis B virus (HBV)-related acute-on-chronic hepatitis B liver failure (ACHBLF) is the most common type of liver failure leading to hepatitis B-related deaths. pFN levels decrease in ACHBLF, and FN levels are significantly higher in surviving patients than in those who die [44].

1.2.5.3. Serum fibronectin distinguishes the early stages of hepatocellular carcinoma

Hepatocellular carcinoma (HCC) accounts for up to 6% of all cancers. HCC is the fifth most common malignancy in men and the ninth in women. It is fatal, and its incidence-to-mortality ratio is very close to one. The average time between its diagnosis and death is

6–20 months [45, 46]. The major risk factors of HCC are Hepatitis B Virus Infection, Hepatitis C Virus Infection, and alcohol. These risk factors can lead to cirrhosis, but the magnitude of HCC risk differs according to the underlying cause of cirrhosis [45]. Among serological biomarkers, alpha-fetoprotein (AFP) is the approved marker for screening HCC. AFP is used for screening and early diagnosis of HCC; however, the sensitivity and specificity of the test are low. Therefore, to improve sensitivity and specificity, another marker is required. It is suggested that both AFP and FN can be used for the early detection of HCC because, compared to liver cirrhosis, serum FN levels are higher in HCC patients [46].

1.2.5.4. Acute liver injury

Acute liver injury, caused by hepatitis virus or hepatotoxins, induces hepatocytes apoptosis and liver damage. After the injury, the liver should be regenerated to restore its function and maintain homeostasis. Liver regeneration needs hepatocytes proliferation and ECM reconstruction. It is reported that FN decreases hepatocyte apoptosis, accompanied by down-regulation of the antiapoptotic protein, B-cell lymphoma—extra-large (Bcl-xL). However, a lack of FN can increase hepatocytes proliferation, which, in turn, surpasses the FN-mediated hepatocyte proliferation activity [47]. Following partial hepatectomy and throughout the regeneration process, the amount of FN messenger RNA (mRNA) rose threefold [48], and FN along with epidermal growth factor (EGF) promote DNA synthesis in primary hepatocyte cultures [49].

1.2.6. Role of fibronectin in bone

The bone ECM consists of minerals (hydroxyapatite) and organic matrix. The main component of the organic matrix is collagen type I. The other constituents of the organic part include osteocalcin, osteonectin, bone sialoprotein, FN, matrix gla-protein (MGP), bone morphogenic proteins (BMPs), growth factors, cytokines, and proteoglycans [50, 51]. FN plays a crucial role in collagen polymerization and maintenance of the bone ECM, and the presence of FN is requisite for collagen type I assembly [52]. Osteoblasts provide the initial FN required for collagen assembly in the early phase of bone formation, but plasma FN is the continuous source of FN in mineralized bone [53].

The amount of FN and collagen increases at the same time in the proliferation phase of osteoblast. Proteins associated with cell phenotype, such as alkaline phosphatase enzyme, rise just after the proliferation phase and at the start of the differentiation and matrix mineralization phase. This implies that osteoblasts are responsible for the assembly of FN during the early phase of bone formation [54]. Moursi et al. have shown that FN is present at the site of osteogenesis, and the addition of anti-FN antibodies to the cultured osteoblasts decreases bone-like nodules creation, which shows the necessity of FN for normal nodule morphogenesis. After removing anti-FN antibodies, cultured osteoblasts resume nodule morphogenesis. The authors concluded that the inhibition is reversible and not cytotoxic [55].

α5β1 integrin is known as FN integrin, or FN receptor. It does not bind to other ECM constituents. FN, however, can bind to 11 different integrins, and osteoblast can express six types of these integrins: α4β1, α5β1, α8β1, αvβ1, αvβ3, and αvβ5 [56, 57]. α5β1 integrin plays a key role in interactions between osteoblasts and FN and it is needed for both bone morphogenesis and osteoblast differentiation [57]. The major source of FN in bone is pFN (from plasma, i.e., hepatocytes) and deletion of pFN (liver-specific FN knockout) results in a reduction of FN in the bone matrix. However, this reduction does not affect bone cells. Although bone mineral density (BMD) is not affected by the deletion of FN made by osteoblast (osteoblast-specific FN knockout), it reduces significantly in the absence of pFN. It was also demonstrated that BMD can increase when pFN is injected into wild type mice [53].

Osteoclast formation consists of two stages. The first stage is the differentiation of hematopoietic cells to pre-osteoclasts, and the second stage is the fusion of pre-osteoclasts into mature multinucleated osteoclasts. FN decreases osteoclast numbers by suppressing the second stage and reduces pre-osteoclast fusion and/or migration. However, a high level of FN can increase osteoclast resorption by increasing the percentage of activated osteoclasts and enhancing their resorptive capacity [58].

1.2.7. Fibronectin role in tooth development and oral tissue

FN is present in gingival cervical fluid. Compared to healthy gingiva, the concentration of FN is lower in the gingival cervical fluid of those having gingival inflammation [59]. Both

intact FN and FN fragments were found in gingival cervical fluid. However, the amount of degraded form in healthy and treated periodontium is higher than in diseased sites having inflammation [60]. Compared to FN fragments (120-kDa cell-binding, 60-kDa heparin-binding, and 45-kDa collagen-binding), intact FN induced greater PDL cell proliferation and chemotaxis [61]. The 40-, 120-, and 68-kDa fragments were highly associated with severe periodontitis sites, and they may have a role in the pathogenesis of periodontal disease [62]. Larjava et al. have shown that plaque and Porphyromonas gingivalis–derived proteases may break intact FN into FN fragments in gingivitis [63].

Histological study on mouth tooth germ revealed that FN could be detected in mesenchymal tissue, basement membranes, and predentin, but FN is not detected in odontoblast and mineralized dentin [64]. FN mRNA expression increases during the presecretory stage in developing dental epithelium, declines in the secretory and early maturation stages and increases during the late maturation phase. FN plays a significant role in the terminal stage of mesenchymal cell differentiation and regulates the elongation and polarization of odontoblasts [65]. FN and enamel protein amelogenin can be detected within similar extracellular compartments during mantle predentine-dentine formation [66]. Epithelial interaction between FN and β1 integrin is essential for ameloblast differentiation and enamel formation [65].

FN increases osteocalcin (OCN) and osteopontin (OPN) gene expression in human dental pulp cells [67]. Surface coating with pFN improves the proliferation, differentiation, and mineralization of odontoblast-like cells by activating β1-integrin (ITGB1) [68]. FN is found with other glycoproteins, such as undulin and tenascin, in normal cementum and PDL [69]. The distribution of FN in the whole normal cementum is uniform from its external surface to the PDL. The direction of FN fibrils in cementum is the same as the direction of collagen fibrils. FN loses its fibrillar morphology or appears amorphous in the recession cementum. FN distribution is also evaluated in periodontally diseased cementum. In the cementum apical to the pocket, FN showed normal fibril structures, similar to the normal one; however, FN showed variation in its distribution and fibrillar structure in the pocket cementum; its absence from the cementum surface is characteristic [70]. FN is present in cultures of human gingival fibroblasts and it may play a role in organization of gingival tissues [71].

1.2.8. Plasma transglutaminase FXIII-A and fibronectin

FN is a major extracellular substrate for FXIII-A [72]. FXIII-A, which is a transglutaminase (TG) enzyme, stabilizes the fibrin network as the last step of the blood coagulation cascade [73, 74]. FXIII-A, as a member of the TG family, catalyzes a calcium-dependent acyl-transfer reaction between polypeptide-bound glutamine residues and lysine residues, resulting in a covalent γ-(glutamyl)-ε-lysyl bond (isopeptide crosslink/bond) that can induce the formation of multimeric protein networks and change the conformation, structure, solubility, biochemical stability, and cell-adhesion properties of substrate proteins [72].

The source of circulating FXIII-A is mostly cells of bone marrow origin, such as megakaryocytes, in contrast to most other clotting factors [75, 76]. FXIII-A is not only present in plasma but also in tissues and is made by a number of cells, including macrophages, chondrocytes, osteoblasts, and osteocytes. It is located in the cytosol and nucleus, on the cell surface, and in the extracellular matrix [77]. It has been shown that FN matrix formation in fibroblasts is enhanced by FXIII-A [78].

In 3T3-L1 and MEF cells, pFN plays an essential role in modulating adipogenesis. FXIII-A acted as a negative adipogenesis regulator by boosting FN assembly from plasma into the preadipocyte extracellular matrix [72]. pFN affects insulin signalling, modulates cell proliferation and differentiation, and controls 3T3-L1 cell adipogenesis [72]. pFN assembly into extracellular matrix is reduced and lipid formation is increased in mouse embryonic fibroblasts lacking FXIII-A [72].

Kaartinen laboratory has shown that two TG family members are expressed by osteoblasts: TG2 and FXIII-A. Among these two, osteoblasts secrete FXIII-A into the extracellular space [79-81]. pFN, but not cFN, functions as an FXIII-A substrate and needs a TG-mediated insolubilization step for its fibrillogenesis. In osteoblast cultures, a lack of pFN or TG activity causes decreased COL I deposition, changes COL I fibril network thickness, decreases alkaline phosphatase activity, decreases lysyl oxidase levels, and reduces mineralization *in vitro*. From this, it appears that pFN assembly in bone is a dynamic, osteoblast-mediated process. Also, pFN and extracellular FXIII-A appear to modulate the quality of COL I matrix produced by mature osteoblasts, whereas cFN

(EDA-FN) appears to control preosteoblast proliferation [82]. Furthermore, our group showed how elevated peripheral extracellular serotonin (5-HT), which is known to regulate bone mass levels may directly impact the stability of pFN matrix network, resulting in the weakening of bone. 5-HT treatment of osteoblast cells significantly reduced pFN fibrillogenesis; this was followed by an increase in pFN levels in the culture medium. 5-HT treatment of osteoblast cultures resulted in a discontinuous pFN matrix and impaired COL I deposition, decreased alkaline phosphatase and lysyl oxidase activity, and delayed mineralization of the cultures [83-86].

1.3. Intraperitoneal route of injection

It is widely acknowledged that the route of administration plays a significant role in determining the ultimate pharmacokinetics, pharmacodynamics, and toxicity of pharmacological drugs. The primary methods of drug administration in laboratory animals are intravenous (IV), subcutaneous (SC), intraperitoneal (IP), and oral. Each has benefits and drawbacks depending on the specific goal(s) of the study [87]. The IP route, which involves injecting a solution into the peritoneal cavity, is one of the commonly used approaches in rodent investigations. This simple method is quick and causes the animals less stress. The intraperitoneal injection is utilized when intravenous or oral administration is inappropriate and relatively large volumes of soluble chemicals need to be rapidly absorbed by small animals [88].

The peritoneal cavity is a closed space within the abdomen, containing the abdominal organs lined by peritoneum, an extensive serous membrane in the body. The peritoneal cavity is filled with a thin layer of peritoneal fluid, which is made up of water, electrolytes, proteins, cells, and other elements derived from the interstitial fluid of the surrounding tissues [87]. Furthermore, the peritoneal fluid has plasma proteins at a concentration of roughly 50% of the amount found in plasma, along with leukocytes, antibodies, and other components needed to fight against infections [89]. In mice, the volume of peritoneal fluid ranges from 0.02 to 0.1 ml [90]. The peritoneum's whole surface is well perfused with blood capillaries, making it an ideal surface for exchanging medications between the peritoneal cavity and plasma [91]. After IP injection, the peritoneal cavity provides a great entry point for substances into the bloodstream. After IP injection, the large surface area

and abundant blood supply allow for quick drug absorption. Additionally, the total transfer from the peritoneal cavity to systemic circulation is considerably facilitated by the lymphatic transport of substrates [92]. A compound must pass through various peritoneal tissues, including the peritoneal fluid, mesothelium, sub-mesothelium, and blood vessel wall, to reach the vascular compartment following IP injection. The primary pathways for solutes and molecules to pass the peritoneal cavity and enter the vascular compartment are transcellular and intercellular spaces in the visceral and parietal mesothelium [93].

1.4. Fluorescent dyes

Fluorescent dyes, also known as fluorophores or reactive dyes, are non-protein compounds that perform by absorbing light at a certain wavelength and reemitting it at a longer wavelength. These compounds have the potential to be used because of their intense fluorescence features. Some factors can quench fluorophores. According to the quenching phenomena, a dye's surroundings significantly impact how brightly it fluoresces. The chemical makeup of the solvent or matrix in which the dye is inserted, as well as the dye's concentration and purity, all impact fluorescence quenching. For instance, molecular oxygen and specific ions can cause significant fluorescence quenching.

A fluorescent dye's absorption and emission spectra often resemble one another's mirror images. Stokes shift is a term used to describe the difference between the wavelength maxima for emission and absorption (**Figure 4**) [94].

2. HYPOTHESIS AND AIMS

Despite of clear contributions of pFN to several tissues and their homeostasis, there have not been any studies examining its accumulation in whole body and comparison between different organs and tissues. This study aims to detect and measure distribution of pFN in the whole body and to develop a method for quantifying and assessing the distribution of a fluorescence-labeled pFN in different organs and tissues of the body. Metabolic tissues were used as a pilot project. The results will open new possible functions for pFN and elaborate on its most relevant roles in whole body function.

3. MATERIALS AND METHODS

3.1. pFN labelling

3.1.1. Protein purification

The protein concentration needs to be at least 2 mg/ml for labeling. Fourteen (14) mg of human plasma FN (Millipore, 1 mg/mL; Catalogue Number: FC010-5MG, FC010-10MG) was purified with Centrifugal Filter Devices (Amicon® Ultra 3K device — 3,000 MWCO, 4 ml, Catalogue Number: UFC800308). After protein purification, 6.2 ml of FN solution remained. All the 6.2 ml of the protein solution were transferred to a dialysis Cassettes (Slide-A-Lyzer™ Dialysis Cassettes, gamma-irradiated, 10K MWCO, 12mL, Thermo fisher, Catalog Number: 66453) and dialyzed twice.

1- dialyzed for 2 hours at room temperature or 4°C, in 1000ml of 100mM NaHCO3 + 500mM NaCl pH 8.4 at 4C.

2- change the dialysis buffer and dialyzed overnight at 4°C, in 1000ml of 100mM NaHCO3 + 500mM NaCl pH 8.4 at 4C.

* Alexa Fluor dyes have NHS esters part and NHS esters are reactive groups created by carbodiimide-activation of carboxylate molecules. NHS ester-activated crosslinkers and labeling compounds react with primary amines in physiologic to slightly alkaline conditions (pH 7.2 to 9) to generate stable amide bonds.

The next day after the two dialyzes, the BSA assay (Micro BCA Protein Assay Kit-Thermo Scientific- Catalog number: 23235) was performed to measure the solution concentration. The protein assay result showed that our solution's concentration is 2.2 mg/ml.

3.1.2. Calculation and preparing buffers for coupling and inactivation of the control:

220000g = 1 mole of FN (220KDa)

13.6 mg of protein = 61.81 nmoles

According to the manufacturer's recommendations, between a quarter and a third of the reactive dye conjugates to the protein, and as the best results are usually obtained with

a DOL between 2 and 5, eight molar excess of dye was utilized. This means we need to add 494.4 nmoles of dye to 13.6 mg of protein (61.81 nmoles).

1 mole of Alexa Fluor 568 = 792g

494.4 nmoles = 0.391 mg

3.1.3. Conjugation of protein

Alexa Fluor 568 NHS Ester (Invitrogen, Catalog number: A20003) was dissolved in DMSO (dimethylsulfoxide) at concentration of 10 mg/ml. Thirty nine (39) µl of the dissolved dye was added to the pFN solution, and Alexa Fluor 568 + pFN solution was incubated at room temperature for one hour with constant and gentle shaking. Because the dye is light sensitive, it was covered with foil. The dye molecules find and attach to proteins via moderate vibration.

3.1.4. Purification of conjugates:

The solution needs to be dialyzed to get rid of the unbound dye. So, the solution was dialyzed twice at 4°C in 1000ml of 100 mM $NaHCO_3$ + 500mM NaCl, pH 8.4 (**Figure 2**). The solution was then transferred to a fresh falcon tube without touching or removing the precipitates. Next, the BCA protein concentration determination was again done, and its result showed that the concentration of Alexa Fluor 568-pFN was 2 mg/ml.

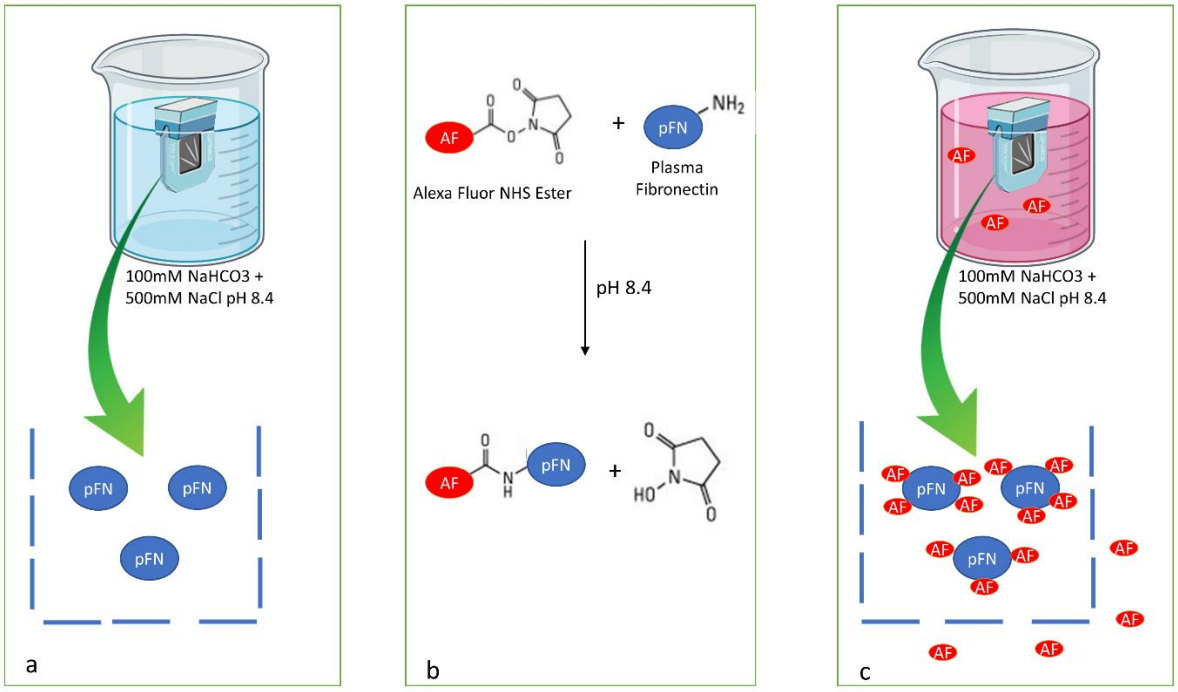

Figure 2. pFN labeling procedure. (a) pFN was dialyzed twice in in 100mM NaHCO3 + 500mM NaCl pH 8.4 at 4C. (b) NHS ester-activated crosslinkers and labeling compounds react with primary amines in physiologic to slightly alkaline conditions (pH 7.2 to 9) to generate stable amide bonds. (c) Because the cut-off size for Dialysis Cassettes is 10 kDa and the molecular weights of pFN and Alexa Fluor are 220 kDa and 1 kDa, respectively, the compound was dialyzed again to remove the unbound Alexa Fluor.

3.1.5. Determination of the degree of labeling:

The relative efficiency of coupling reaction can be assessed by measuring the absorbance of the protein at λ=280 nm and the absorbance of the dye at its absorbance maximum (λmax). According to the Lambert-Beer law A = C x path length (usually 1 cm) x ε, with C = concentration (M) and ε = extinction coefficient (cm-1 x M-1), the concentration of protein and the bound fluorophore can be calculated as follows.

Dye	λmax (nm)	Em (nm)	E (cm–1 M–1)	CF280
Alexa Fluor® 568	578	603	91,300	0.46

The absorbance of the protein has to be corrected by the absorbance of the fluorophor at λ=280 nm, which is expressed as correction factor Cf 280 (A280 free fluorophor/Amax).

The correction factor for the Alexa Fluor 568 is 0.46.

$$C\ protein = \frac{A280 - (Amax \times Cf\ 280)}{\varepsilon protein}$$

$$C\ fluor = \frac{Amax}{\varepsilon fluor}$$

With this formula, the degree of labeling (DOL, i.e., moles fluorophor per mol protein, D/P) can be calculated:

$$DOL = \frac{Cfluor}{Cprotein} = \frac{Amax * \varepsilon protein}{\varepsilon fluor \times [A280 - (Amax \times Cf\ 280)]}$$

To get a more accurate OD, the Alexa Fluor 568- pFN solution was diluted 10X using 100 mM NaHCO3 + 500mM NaCl, pH 8.4.

A280 of the 10X diluted sample was 0.158.

Amax = A578 for Alexa Fluor 568 (absorbance at absorbance maximum of the dye i.e., 568 (λmax))

A568 = 0.099

εfluor = 91,300 cm-1 M-1 as mentioned on Alexa Fluor 568 datasheet.

εprotein = 1.3 cm-1 (mg/ml)-1 or 364560 cm-1 M-1

$$C\ protein = \frac{A280 - (Amax \times Cf280)}{\varepsilon protein} = \frac{0.158 - (0.099 \times 0.46)}{364560} = 308 \times 10^{-9}\ M$$

$$C\ fluor = \frac{Amax}{\varepsilon fluor} = \frac{0.099}{91300} = 1084 \times 10^{-9}\ M$$

$$DOL = \frac{Cfluor}{Cprotein} = \frac{1084 \times 10^{-9}\ M}{308 \times 10^{-9}\ M}$$

DOL = 3.51

3.1.6. Inactivation of dye for control

For the control group, the dye was inactivated with Tris (9 mg of protein = 40.9 nmoles) (40.9*3.5= 143.15 nmoles (the amount of needed dye) = 113.37 mg)

The degree of labeling was 3.5. As a result, 0.113 mg of dye was used. Dye was added into 4.5 ml of 50mM tris +500mM NaCl solution pH 8.0. It was incubated at room temperature for one hour with constant and gentle shaking.

3.1.7. Confirmation of labelling and pFN assembly to matrix in cell culture

3T3-L1 Mouse embryonic fibroblasts (MEFs) cells were grown in 8-well Nunc Lab-Tek® II glass chamber slides (Fisher Scientific). Labeled pFN was added to the media on day 7, and the slides were prepared after 24 hours. Cells were washed and fixed with 3.7% formalin for 10 min at room temperature (RT), followed by permeabilization with 0.25% Triton X 100 for 10 min. Cells were then blocked with 2% BSA. DAPI was used to stain the nuclei, and images were taken under 20 X objective. A microscope (AxioImager M2; Zeiss) was used to capture immunofluorescence images with an Orca Flash 4.0 camera.

3.1.8. Determining the amount and volume for injection

The volume of the IP injection was set to 20 ml/kg body weight, which is the maximum volume approved by McGill University's Animal Policy and Welfare Oversite Committee in the standard operating procedure for substance administration. In this experiment, 12 weeks old C57/bl6 male mice were used. The mice were categorized into two groups (each group contained 3 mice).

The concentration of pFN - labeled Alexa Fluor 568 solution was 2 mg/ml. 0.5 ml of pFN - labeled Alexa Fluor 568 solution (equal to 1mg pFN) was injected intraperitoneally into each mouse for three consecutive days (**Figure 3**) [53, 95]. Inactivated Alexa Fluor 568 was injected into the control group. During repeated injections, injection sites were alternated. After 24 hours of the last injection, the mice were euthanized by CO_2 asphyxiation under isoflurane anesthesia.

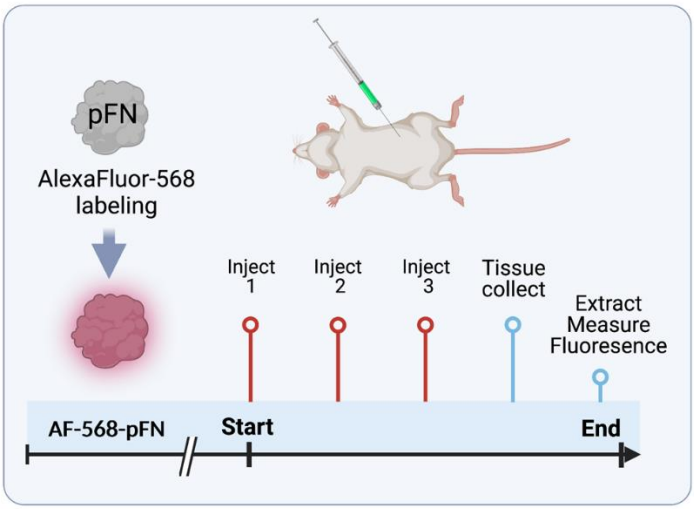

Figure 3. Labeled pFN administration. For three days in a row, each mouse received an intraperitoneal injection of 1 mg of labeled pFN. The control group received an injection of inactive AF. The mice were euthanized 24 hours after the final injection.

3.2. Mouse dissection

The mice were euthanized, and tissues were stored in -80 c.

List of analyzed tissues:

1- Liver
2- Kidney
3- Pancreas
4- Intestine
5- Adipose tissue (SAT)
6- Adipose tissue (VAT)
7- Adipose tissue (BAT)
8- Tail

9- Testis
10- Heart
11- Bone marrow
12- Skin
13- Skeletal muscle
14- Serum

3.3. Protein extraction

The RIPA-SDS/DOC buffer with protease inhibitor was used for protein extraction. RIPA buffer (150mM NaCl, 10mM Tris-HCl, 5mM EDTA, 0.1 % SDS, 1.0 % Triton X-100, 1.0 % Na-Deoxycholate PH 7.2) was prepared freshly before protein extraction. Protease inhibitor cocktail (1:100) and the phosphatase inhibitor (1:100) were added just before protein extraction. Tissues were dissected and washed briefly with chilled PBS to remove any blood. Then, tissues were cut into smaller pieces while keeping them on ice.

For every 10 mg of tissue, 500 µl RIPA buffer was added. Samples were sonicated to enhance the extraction. Samples were centrifuged at 10,000 x g for 20 minutes at 4°C to pellet cell debris. After that, Supernatants were transferred to tubes, and BCA assay was performed to determine protein concentration.

3.4. pFN matrix quantification via fluorometer

Each sample (150 µ)l was loaded in the 96-well black plate (Thermo Scientific™- Catalog number: 237108) in triplicate. (For each sample, a total of 450 µl was loaded into three wells). To draw a standard curve, a different concentration of Alex Fluor 568-pFN was added to RIPA buffer, and 150 µl of each standard was loaded in a well in triplicate.

The plate was read with Fluorometric Plate Reader (Infinite 200) from the top. The excitation and emission wavelengths of the fluorometer's filter were 560nm and 610nm, respectively. Furthermore, the fluorometer's excitation and emission bandwidths were 10 nm and 20 nm, respectively (**Figure 4**).

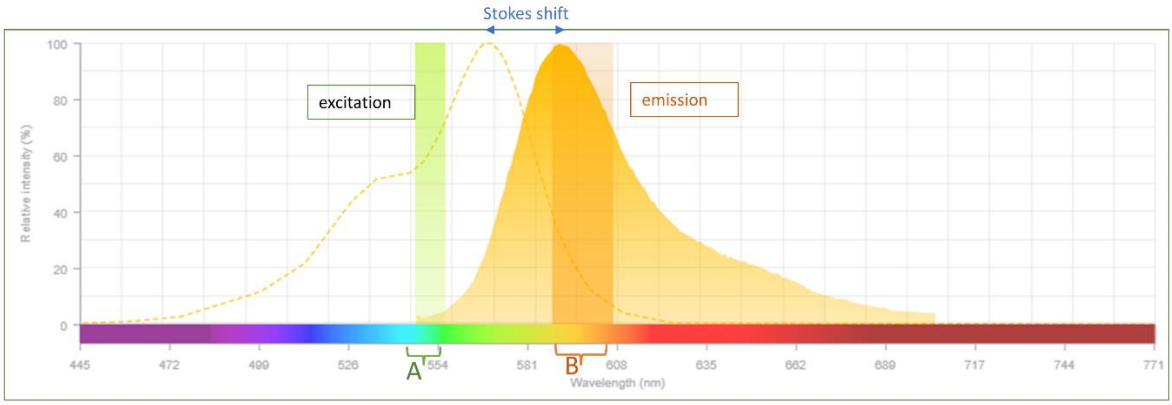

Figure 4. excitation and emission spectra of the fluorophore. The two bell shape graphs are the excitation and emission wavelength of Alexa Fluor 568. Alexa Fluor 568's excitation and emission wavelengths are 578 and 602 nm, respectively. The filter fluorometer's excitation and emission wavelengths were 560 nm and 610 nm, respectively. The fluorometer's excitation and emission bandwidths were 10 nm and 20 nm, respectively. A and B show the wavelength range read by the fluorometer.

3.5. Calculating the quantity of each sample's labeled plasma fibronectin

The standard curve was drawn based on the result of standard solutions.

The standard solution and its concentration were as below:

1- RIPA buffer (blank solution)
2- AF 568 pFN in RIPA solution (0.1 µg/ml)
3- AF 568 pFN in RIPA solution (0.5 µg/ml)
4- AF 568 pFN in RIPA solution (2 µg/ml)
5- AF 568 pFN in RIPA solution (4 µg/ml)
6- AF 568 pFN in RIPA solution (6 µg/ml)
7- AF 568 pFN in RIPA solution (10 µg/ml)
8- AF 568 pFN in RIPA solution (13 µg/ml)

Based on the standard curve, the quantity of labeled pFN in each sample was calculated. Next, the total amount of pFN was divided by the total amount of proteins. In this way, we can determine how much labeled pFN there is in the tissue as per protein.

3.6. Detecting labeled pFN with fluoroimager

The BCA assay was done to determine the protein concentration in the plasma of labeled pFN and control (inactivated Alexa Fluor) groups. Each sample (20 µg) was taken, and equal volume 2X Laemmli sample buffer was added. The solutions were boiled at 95 °C for 5 min to denature the proteins. An equal amount of protein (20 µg) was loaded into the wells of the SDS-PAGE gel. The last well was loaded with a prestained molecular weight ladder. The gel ran for one hour at 100 V. Because FN is a large-weight protein, the 10% gradient gel was utilized. Following that, the gel was taken out of its cassette and read with a Fluoroimager (Typhoon 8600). The Ex-wavelength was 532nm and the Em filter used was the 610BP30 (this means the filter is only allowing emission wavelengths of 610nm +/- 30nm to be detected).

3.7. Visualization of pFN matrix under fluorescence microscopy

In the second experiment, pFN was labeled with Alexa Fluor 680. In this experiment, 12-week-old C57/bl6 male mice were used and divided into two groups (there were 3 mice in each group). The labeled pFN was injected intraperitoneally into 3 mice, and in the control group, the inactivated Alexa Fluor was injected. For three days in a row, each mouse received an intraperitoneal injection of 1 mg of labeled pFN. Inactivated AF 680 was injected into the control group (**Figure 3**). After 24 hours of the last injection, the mice were euthanized by CO2 asphyxiation under isoflurane anesthesia, and tissues were harvested.

3.8. Histology analysis

The tissues were prepared in 3 distinct methods for histological analysis:

1- Traditional Paraffin Embedding Technique: The tissues were fixed in 4% paraformaldehyde for 24 h. The tissue was subsequently dehydrated using a graded series of ethanol solutions (five solutions were used: 50, 75, 95, 100, and 100%, v/v). After dehydration, the samples were ready for infiltration. They were successively immersed in a graded series of infiltration solutions (50% in 100% ethanol and 100% in 100% xylene). Then, samples were submerged in paraffin [96] and sectioned (6 µm). Sections were deparaffinized in xylene and rehydrated with decreasing ethanol

concentrations in H_2O. In the next step, sections were treated with protease XXIV for antigen retrieval and then washed with a solution of TBS containing 0.05% Tween 20. The sections were then blocked with 2% BSA in TBS for 1h at room temperature. Next, sections were counterstained with Alexa Fluor 488 phalloidin (Thermo Fisher #A12379) and cell nuclei were visualized with 4',6-diamidino-2- phenylindole, dihydrochloride (DAPI) to better define tissue structure.

2- **TBA-Dehydrating Paraffin Embedding:** The tissues were fixed in 4% paraformaldehyde for 24 h. The tissue was subsequently dehydrated using a graduated series of TBA solutions (five solutions were used: 50, 75, 95, 100, and 100%, each incubated for 12 h at 30°C). After dehydration, the samples were immersed in paraffin at 60°C for 12 h [96] and sectioned 6 µm thickness. Sections were deparaffinized in xylene and rehydrated with decreasing ethanol concentrations in H_2O. In the next step, sections were treated with protease XXIV for antigen retrieval and then washed with a solution of TBS containing 0.05% Tween 20. The sections were then blocked with 2% BSA in TBS for 1h at room temperature. Next, sections were counterstained with Alexa Fluor 488 phalloidin (Thermo Fisher #A12379) and cell nuclei were visualized with 4',6-diamidino-2- phenylindole, dihydrochloride (DAPI) to define tissue structure better.

3- **Frozen Embedding:** The tissues were fixed in 4% paraformaldehyde for 2 h. The tissues were then cryoprotected by incubating in a 30% sucrose solution and then embedded in OCT compound (optimal cutting temperature compound) [35]. Cryosections were cut at 8µm thickness and hydrated in TBS. Slides were immersed in TBS+ 0.05% Tween 20 For permeabilization and intracellular protein staining and then blocked with 2% bovine serum albumin (BSA). Next, sections were counterstained with Alexa Fluor 488 phalloidin (Thermo Fisher #A12379), and cell nuclei were counterstained with 4',6-diamidino-2- phenylindole, dihydrochloride (DAPI) to better illustrate tissue structure.

Figure 5 provides an overview of these techniques.

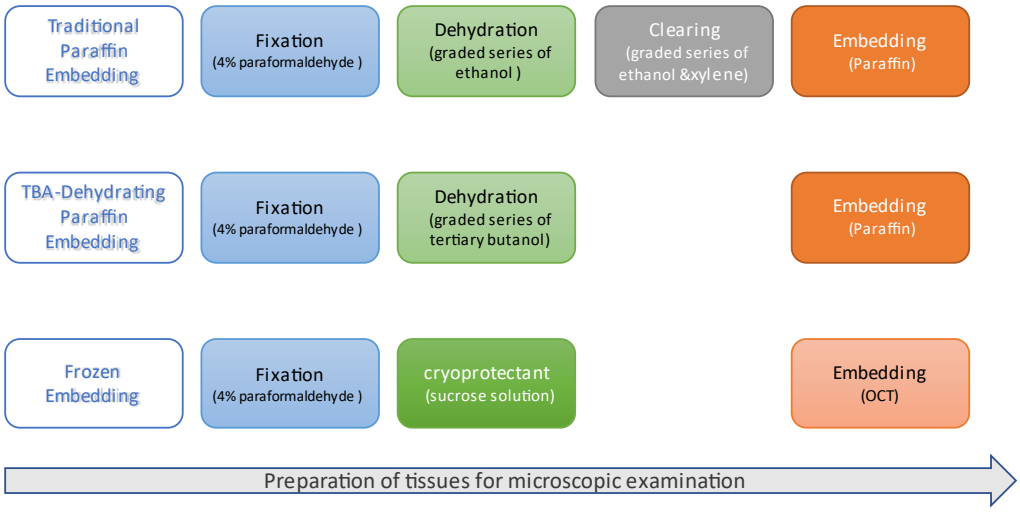

Figure 5. Overview of different methods used to prepare slides. There is no dehydration step in the Frozen Embedding technique.

3.9. Light microscopy Imaging

An epifluorescence microscope (AxioImager M2; Zeiss) was used to capture immunofluorescence images with an Orca Flash 4.0 camera. The slides were analyzed with a Cy5 filter set. The same settings were used to capture photos of the control and pFN-treated groups in each tissue.

3.10. Analysis of immunofluorescence images

Standard deviation and average gray value (sum of the gray values of all the pixels in the selection divided by the number of pixels) of each slide were calculated using ImageJ. Next, data were analyzed with GraphPad Prism software (version 5.0). The unpaired Student's Ttest was used to compare the control and AF 680 pFN group. The α was set at 0.05 and p-values < 0.05 were considered statistically significant (*: $p < 0.05$, **: $p < 0.01$, ***: $p < 0.001$, ****: $p < 0.0001$).

3.11. Statistical analysis

Data were analyzed with GraphPad Prism software (version 5.0). For comparisons of the control and AF 568 pFN group for each tissue separately, Student's Ttest was used. Results were graphed as mean values of three independent replicate experiments, with error bars corresponding to standard error of the mean (SEM). The α was set at 0.05 and p-values < 0.05 were considered statistically significant (*: $p < 0.05$, **: $p < 0.01$, ***: $p < 0.001$).

4. Results

4.1. pFN labeled with Alexa Fluor 568 assembles into matrix fibrils

To examine whether Alexa Fluor labeling was successful and to confirm that labeled pFN can form FN matrices, different concentrations of AF 568 pFN (10 µg and 5 µg) were added to MEF cell cultures which are known to assemble FN matrix. The equivalent amount of Alexa Fluor dye, which was inactivated with Tris, was added to other wells of chamber slide. After 24 hours, the slides were prepared (**Figure 6**). The formation of the FN matrix in the cultures is obvious in the wells containing 10 µg of Alexa Fluor 568-pFN and Alexa Fluor 680-pFN. In the wells treated with 5 µg of Alexa Fluor 568,680 pFN, the FN matrix was visible but compared to the cells treated with 10 µg AF pFN, the amount of FN matrices decreases (data not shown). There was no evidence of FN matrix formation in the control group, which shows that Alexa Fluor dye had successfully labelled pFN and labelled-pFN can form matrices.

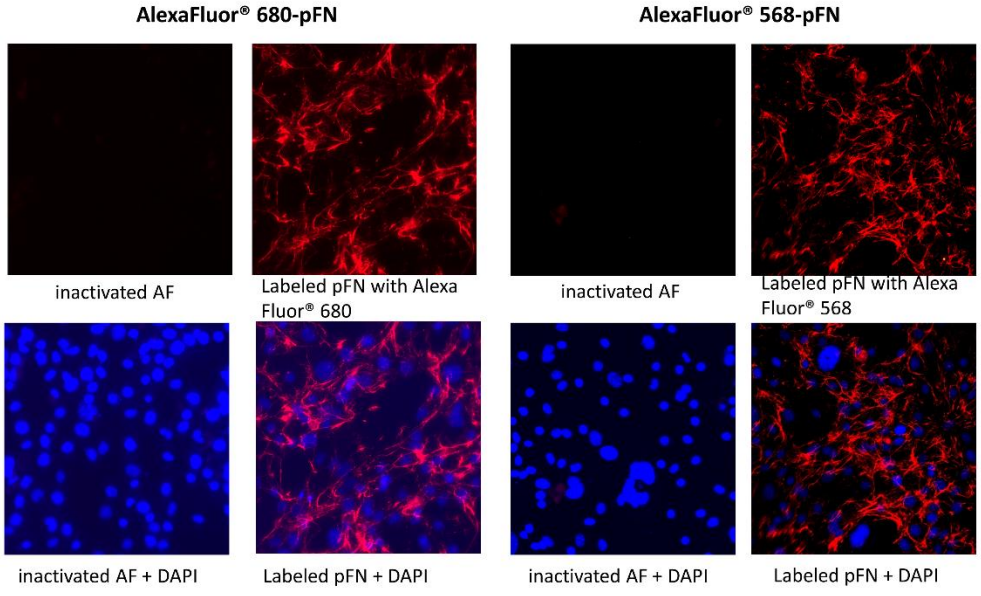

Figure 6. pFN matrix network in cell culture. IF staining for visualizing AF pFN matrices in Mouse Embryonic Fibroblasts. Images were taken under 20 X objective. In both AF568 pFN and AF680 pFN, the formation of FN matrices in the group treated with 10 µg AF pFN is evident.

4.2. The labeled pFN was detected in the plasma.

Fluoroimager results show that labeled pFN can be seen in SDS-PAGE gel, indicating that labeled pFN entered the systemic circulation from the peritoneal cavity, and remained intact as a protein (**Figure 7**).

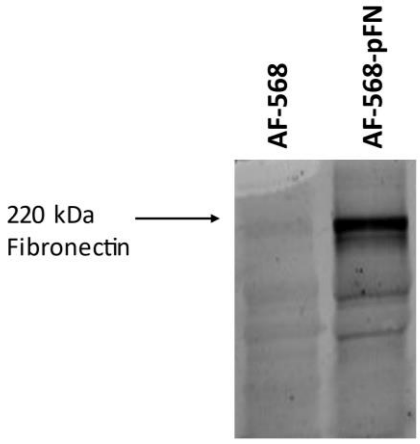

Figure 7. Injected AlexaFluor-568 labeled pFN is found in mouse plasma.
Intraperitoneal injections of AF-568 labeled pFN result in its abundant presence in plasma as analyzed by fluoroimaging of an SDS-PAGE gel. Control group plasma (AlexaFluor568 injected) does not show any fluorescence signal in plasma.

4.3. pFN protein accumulates in all tissues measured

The Alexa Fluor 568-pFN fluorescence signals were read using a fluorometer to quantify and analyze levels of Alexa Fluor 568-pFN in various tissues. Fluorometer data and signal from all tissues were gathered and divided by the total amounts of proteins in each tissue. Nearly all tissues had significantly stronger fluorescence signals in the pFN-injected group than in the control group. This shows that labeled pFN enters many tissues from plasma. These differences between the control and pFN injected groups are very significant in visceral adipose tissue (VAT). The difference between the two groups in plasma, liver, bone marrow, and subcutaneous adipose tissue is also high (**Figure 8**). Skin appears as

only tissue where there was no significant difference between labelled-pFN and dye alone signals.

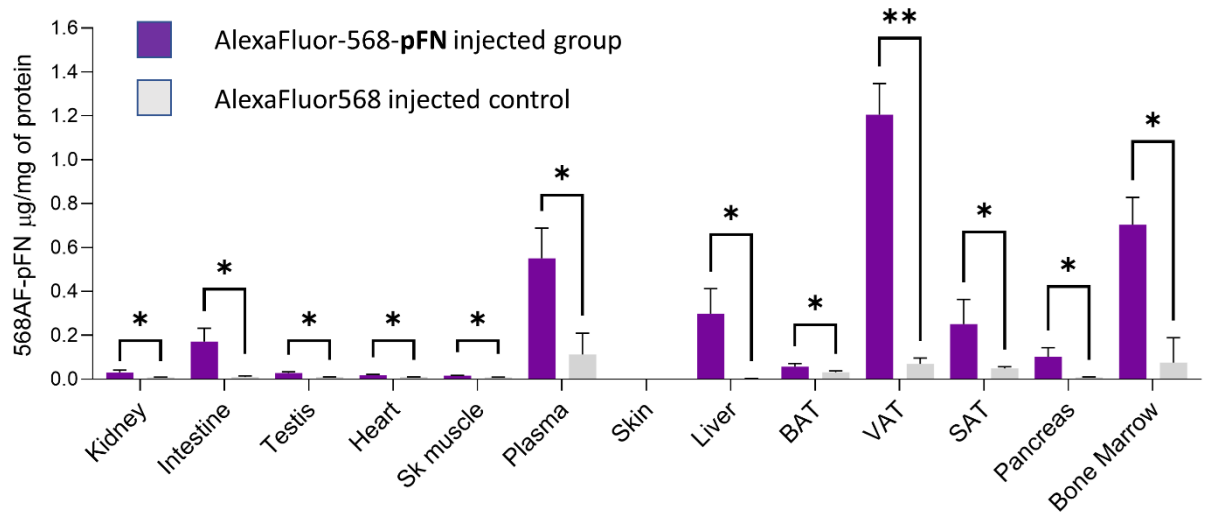

Figure 8. The fluorescence signal based on the amount of protein in each tissue in the control and pFN injected group. Almost all tissues exhibit a significant difference between the two groups. This difference is noticeable in visceral adipose tissue, plasma, liver, bone marrow, and subcutaneous adipose tissue.

4.4. Highest labeled pFN levels are detected in Visceral Adipose Tissue, Bone Marrow, and Liver

Control solutions were considered blank solutions to eliminate the background signal, and the concentration of labeled pFN in each sample was calculated after drawing the standard curve. The quantification (**Figure 9**) indicates that visceral adipose tissue (VAT) had the highest concentration of labeled pFN per 1 mg of total protein. The next highest concentration was found in the following tissues: bone marrow, plasma, liver, gut, pancreas, brown adipose tissue, heart, tail, kidney, testis, and skeletal muscle. Based on **Figures 8 and 9**, skin appears not to accumulate any pFN. The concentration of labeled

pFN based on the weight and volume of tissues is also calculated in **Figures 10 and 11**, respectively.

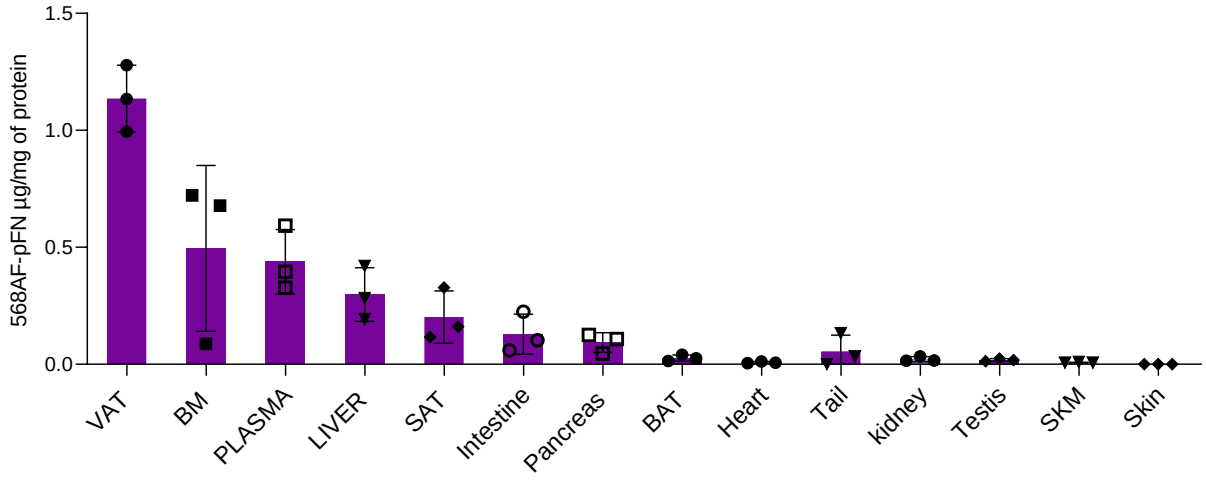

Figure9. The concentration of labeled pFN per 1mg of protein in different tissues. The highest amount of labeled pFN per 1 mg of protein is seen in visceral adipose tissue.

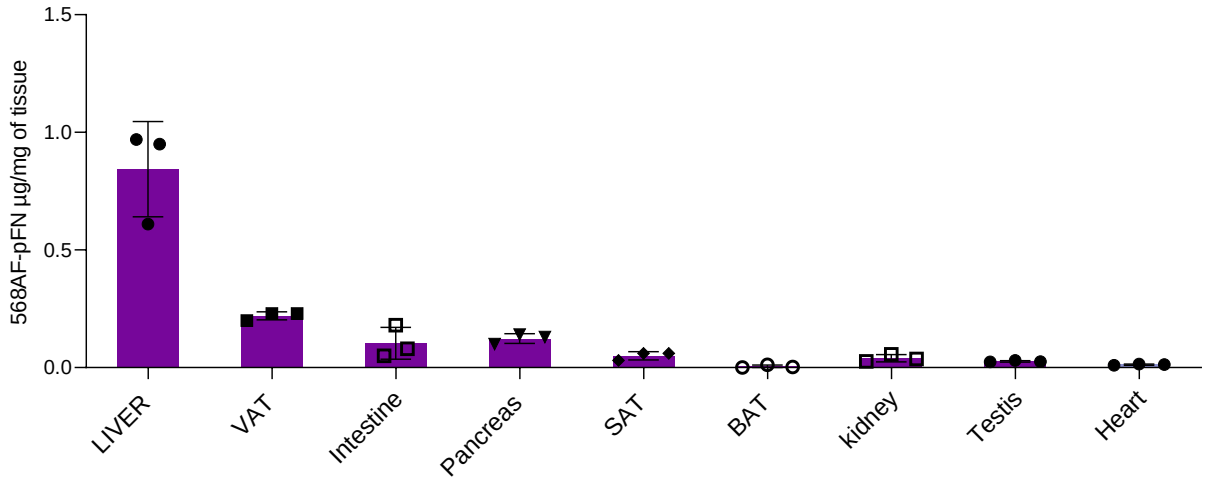

Figure 10. The concentration of labeled pFN in 1 mg of different tissues. This graph is sorted based on the tissue weight. The liver has the highest concentration of labeled pFN.

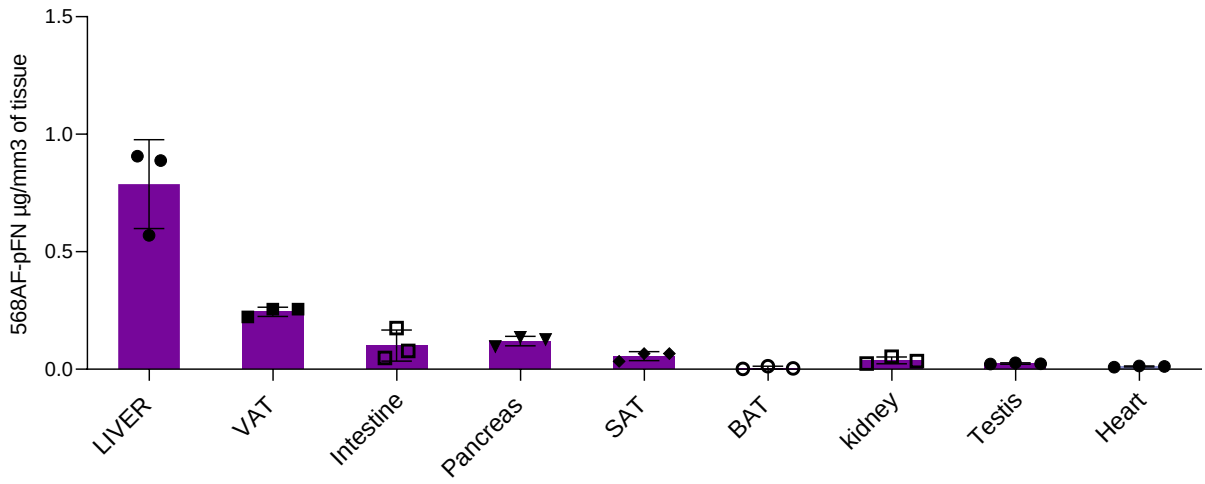

Figure 11. The concentration of labeled pFN in 1 mm^3 of different tissues. This graph is sorted based on the tissue volume. The liver has the highest concentration of labeled pFN.

4.5. Fluorescence microscopy

The three different methods used to prepare the slides are listed below:

1- Traditional Paraffin Embedding Technique

2- TBA-Dehydrating Paraffin Embedding

3- Frozen Embedding

The brightness of a pixel is indicated by the grey value or level. In these images, the level of gray value is used to compare the control group with the labeled pFN group. Although the level of grey value in the labeled pFN group is higher than the control group in all samples, the signals are weak.

The difference between the control and pFN groups in the liver is entirely evident in the frozen embedding technique (**Figure 12**).

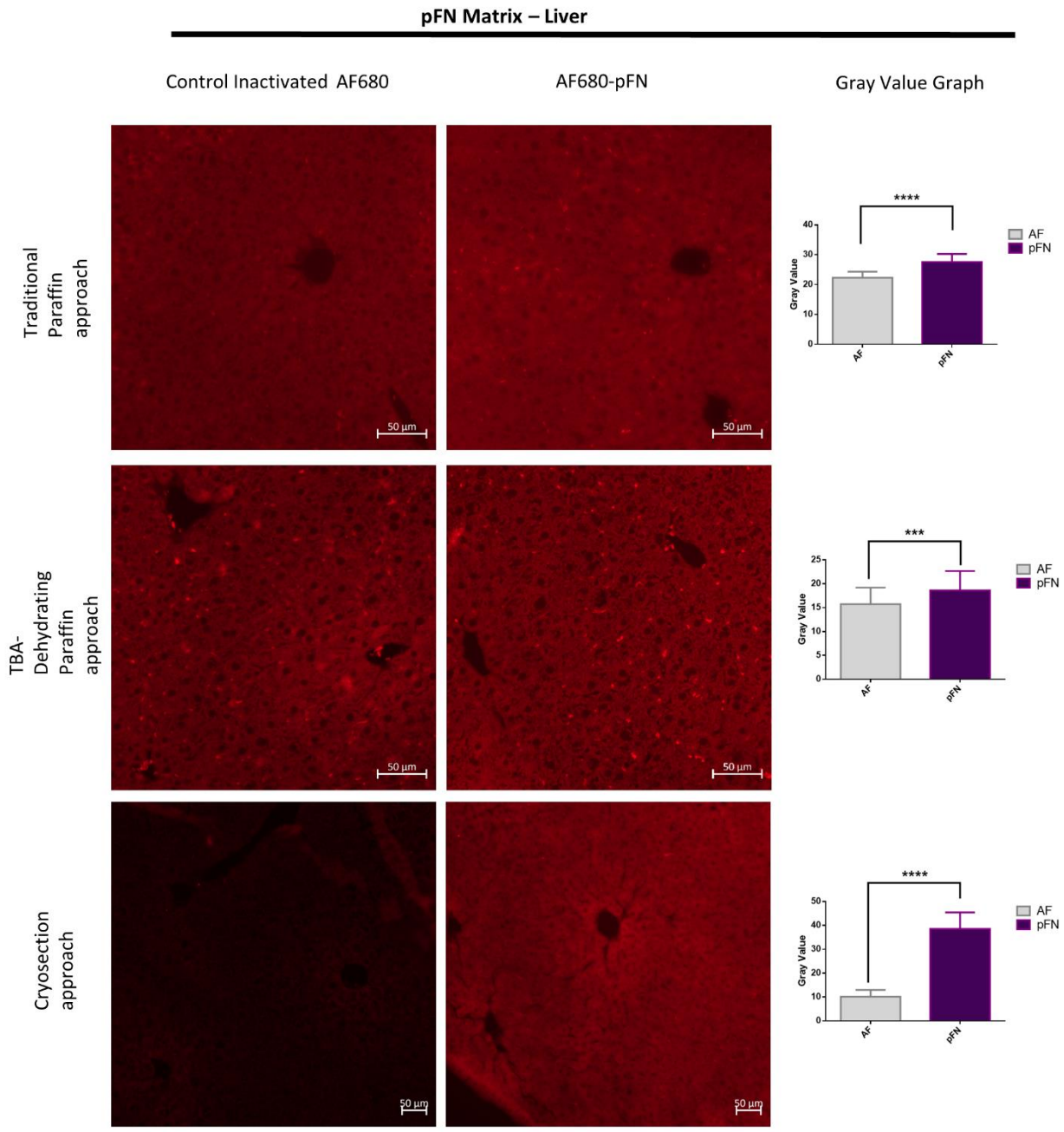
pFN Matrix – Liver
Control Inactivated AF680
AF680-pFN
Gray Value Graph
Traditional Paraffin approach
TBA-Dehydrating Paraffin approach
Cryosection approach
50 µm
****
***
Gray Value
AF
pFN

Figure 12. Detection of AlexaFluor-680-pFN matrix in the liver. Three different methods were used for preparing the slides. The mean gray value intensity in all methods is higher in the AF680-pFN group compared to the control one, but the difference in the frozen embedding technique is more apparent. The tissue area was selected, and standard deviation and average gray value (sum of the gray values of all the pixels in the selection divided by the number of pixels) of each slide were measured using ImageJ. Next, data were analyzed with GraphPad Prism software. The unpaired Student's Ttest was used to compare the control and AF 680 pFN group. The α was set at 0.05 and p-values < 0.05 were considered statistically significant (*: $p < 0.05$, **: $p < 0.01$, ***: $p < 0.001$, ****: $p < 0.0001$). The same settings were used to capture and analyze photos of the control and pFN-treated groups in each approach.

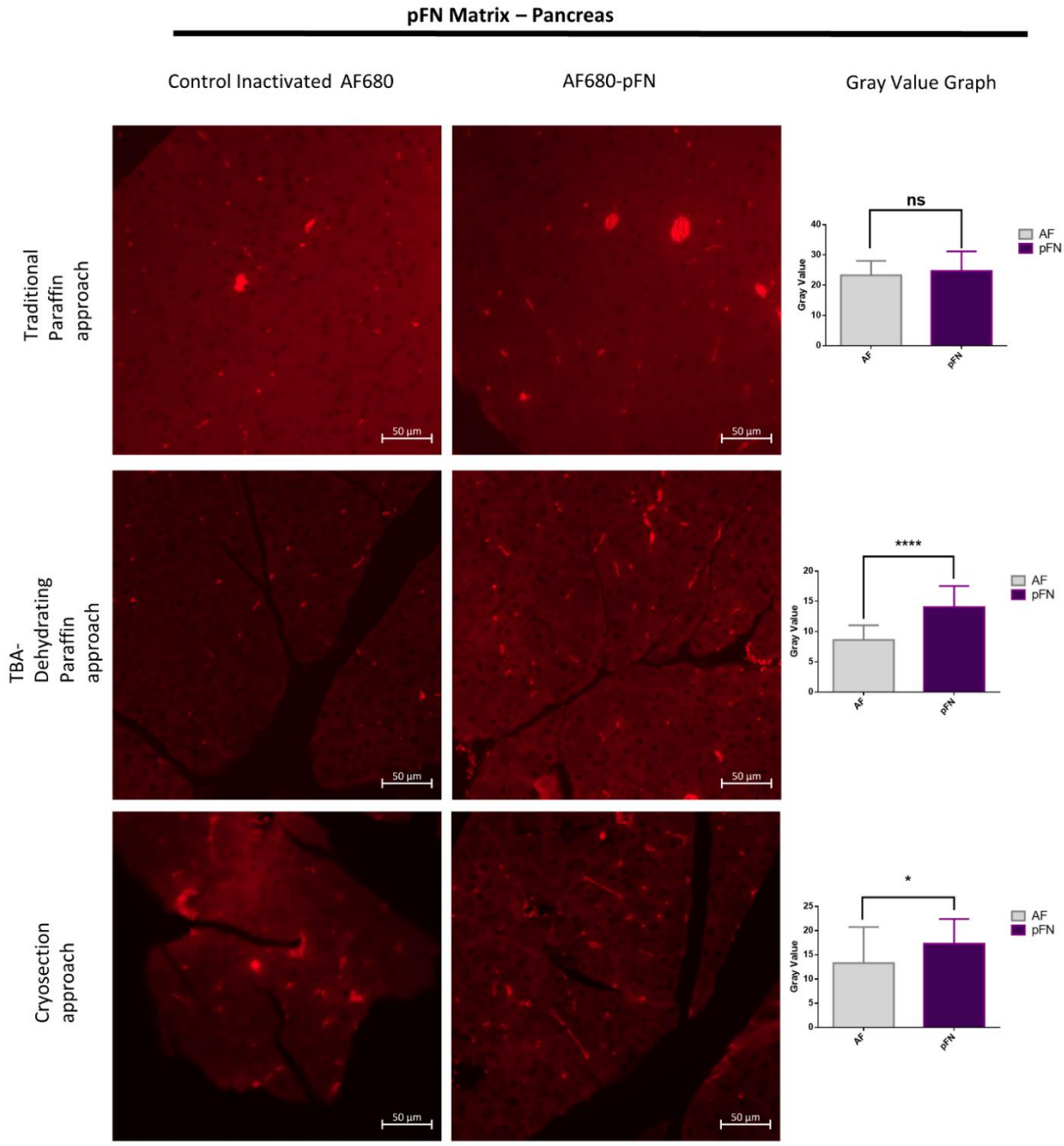
pFN Matrix – Pancreas
Control Inactivated AF680
AF680-pFN
Gray Value Graph
Traditional Paraffin approach
TBA-Dehydrating Paraffin approach
Cryosection approach
50 µm
ns
****
*
Gray Value
AF
pFN

Figure. 13. Detection of AlexaFluor-680-pFN matrix in the pancreas. Three different methods were used for preparing the slides. In the TBA-Dehydrating Paraffin Embedding and Frozen Embedding technique, the difference between the control and AF680-pFN group is significant, but in Traditional Paraffin Embedding Technique, the difference is not significant. The tissue area was selected, and standard deviation and average gray value (sum of the gray values of all the pixels in the selection divided by the number of pixels) of each slide were measured using ImageJ. Next, data were analyzed with GraphPad Prism software. The unpaired Student's Ttest was used to compare the control and AF 680 pFN group. The α was set at 0.05 and p-values < 0.05 were considered statistically significant (*: $p < 0.05$, **: $p < 0.01$, ***: $p < 0.001$, ****: $p < 0.0001$). The same settings were used to capture and analyze photos of the control and pFN-treated groups in each approach.

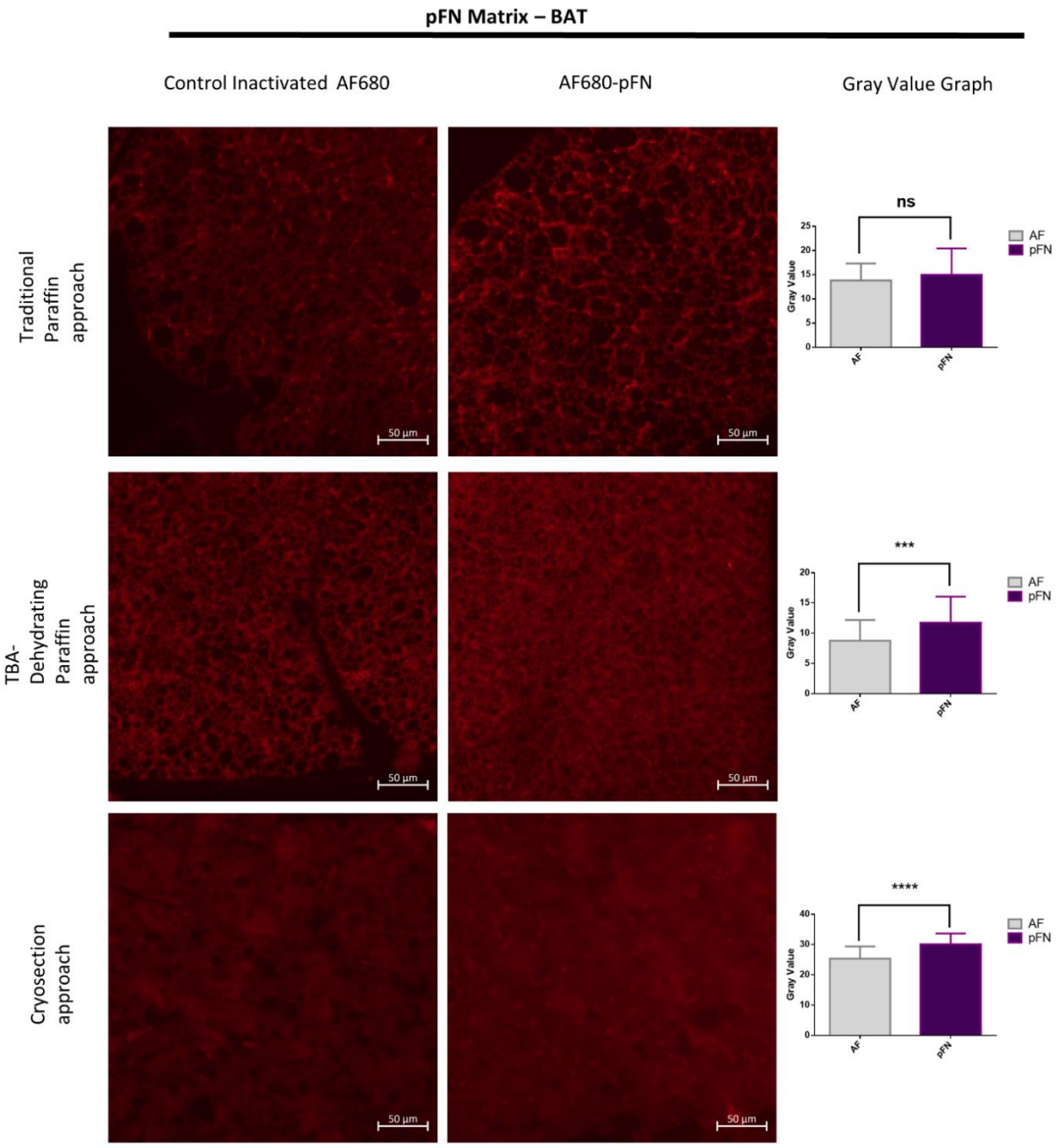
pFN Matrix – BAT
Control Inactivated AF680
AF680-pFN
Gray Value Graph
Traditional Paraffin approach
TBA-Dehydrating Paraffin approach
Cryosection approach
50 µm
ns
***
****
Gray Value
AF
pFN

Figure 14. Detection of AlexaFluor-680-pFN matrix in the Brown adipose tissue. In all methods, the gray value level is higher in the AF680-pFN group compared to the control group, but this difference is not significant in Traditional Paraffin Embedding Technique. The tissue area was selected, and standard deviation and average gray value (sum of the gray values of all the pixels in the selection divided by the number of pixels) of each slide were measured using ImageJ. Next, data were analyzed with GraphPad Prism software. The unpaired Student's Ttest was used to compare the control and AF 680 pFN group. The α was set at 0.05 and p-values < 0.05 were considered statistically significant (*: $p < 0.05$, **: $p < 0.01$, ***: $p < 0.001$, ****: $p < 0.0001$). The same settings were used to capture and analyze photos of the control and pFN-treated groups in each approach.

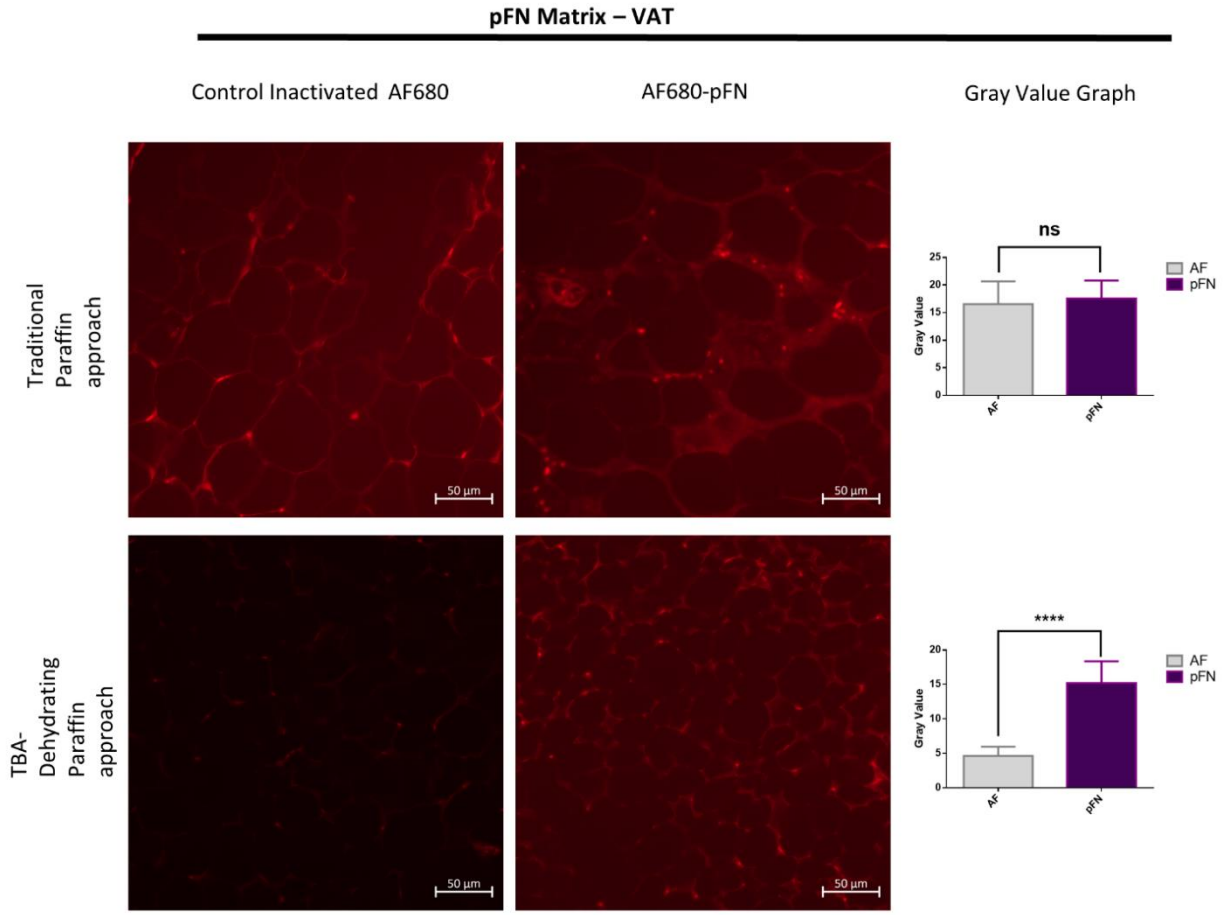

Figure 15. Detection of AlexaFluor-680-pFN matrix in the visceral adipose tissue. There is a significant difference between the two groups in the TBA-Dehydrating Paraffin Embedding technique. The tissue area was selected, and standard deviation and average gray value (sum of the gray values of all the pixels in the selection divided by the number of pixels) of each slide were measured using ImageJ. Next, data were analyzed with GraphPad Prism software. The unpaired Student's Ttest was used to compare the control and AF 680 pFN group. The α was set at 0.05 and p-values < 0.05 were considered statistically significant (*: $p < 0.05$, **: $p < 0.01$, ***: $p < 0.001$, ****: $p < 0.0001$). The same settings were used to capture and analyze photos of the control and pFN-treated groups in each approach.

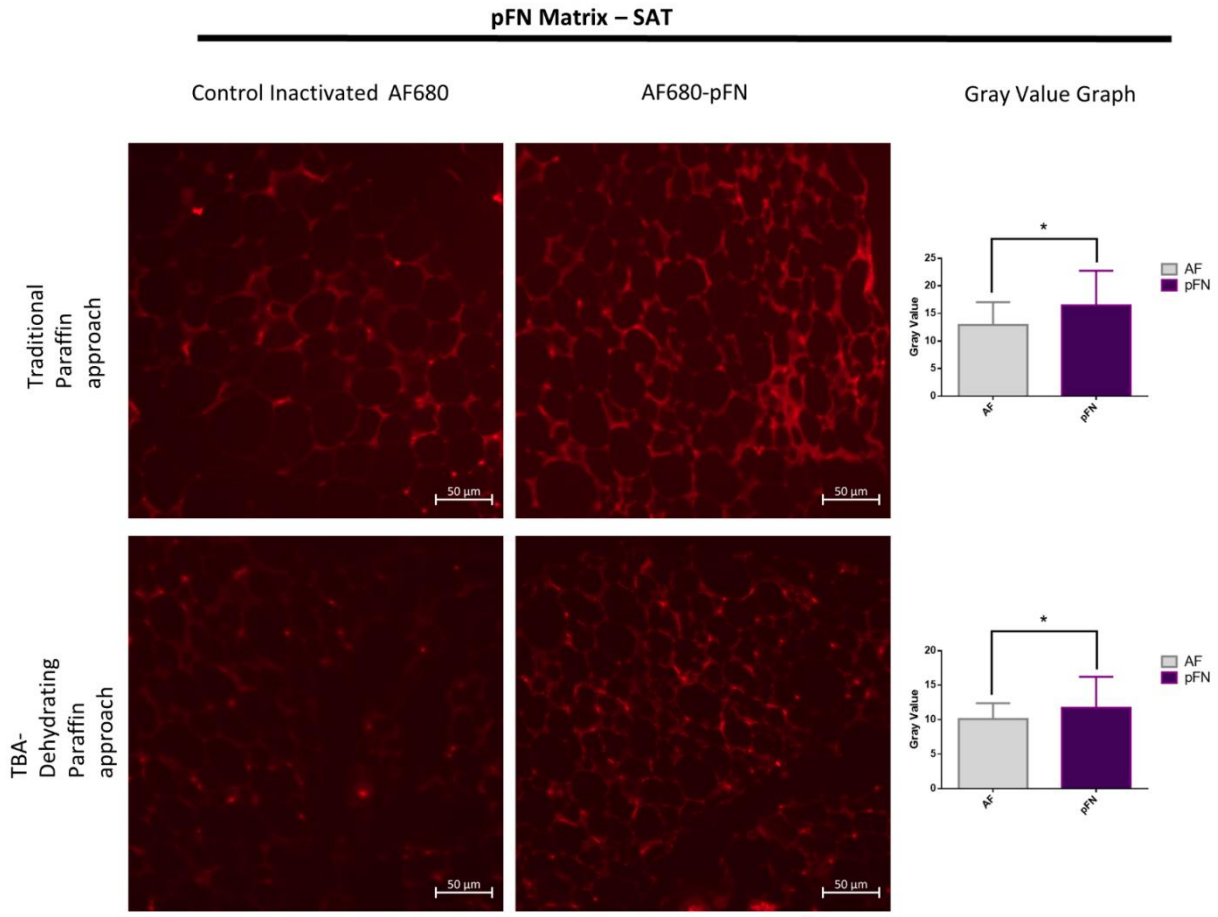

Figure 16. Detection of AlexaFluor-680-pFN matrix in the Subcutaneous adipose tissue. The level of gray value is higher in the AF680-pFN group compared to the control group in both TBA-Dehydrating and Traditional Paraffin Embedding Technique. The tissue area was selected, and standard deviation and average gray value (sum of the gray values of all the pixels in the selection divided by the number of pixels) of each slide were measured using ImageJ. Next, data were analyzed with GraphPad Prism software. The unpaired Student's Ttest was used to compare the control and AF 680 pFN group. The α was set at 0.05 and p-values < 0.05 were considered statistically significant (*: $p < 0.05$, **: $p < 0.01$, ***: $p < 0.001$, ****: $p < 0.0001$). The same settings were used to capture and analyze photos of the control and pFN-treated groups in each approach.

5. Discussion

FN is a multifunctional ECM protein that mediates a wide range of cellular interactions between cells and their environment, including cell adhesion, migration, proliferation, and differentiation. Altered levels of circulating pFN have been seen in a variety of illnesses, such as cancer [97], different stages of liver disease [98-100], diabetes [101], coronary heart disease [74, 102], and periodontal disease [59]. In these pathological conditions, pFN may act as a biomarker and disease modifier. Although pFN is the source of a significant amount of tissue FN, little is known about how it is distributed throughout the body. Knowing the distribution of pFN in the body and its accumulation in different tissues can help us explain why the level of pFN in serum changes in different diseases. Furthermore, the findings of this study can open new possible functions for pFN and elaborate on its most relevant roles in whole-body function.

Our aim in this study is to develop a method for analyzing pFN accumulation in different tissues and its distribution throughout a mouse's body. Metabolic tissues were used as a pilot project in this study. In order to quantify and see the pFN, the first step was labeling it with a fluorophore. AlexaFluor-568-pFN and AlexaFluor-680-pFN formed ECM fibrils in MEF cultures, which shows that fluorophore formed a stable bond with pFN, and labeled pFN can form a matrix in ECM. After labeling, we used different methods to measure the quantity of pFN by measuring the fluorescence signal. The labeled FN and inactive Alexa Fluor were injected intraperitoneally. FN has a molecular weight of 220 kDa, whereas inactive Alexa Fluor has a molecular weight of roughly 1200 Da. Small to medium-sized molecules (MW 5000) and fluids are mostly taken up by diffusion through the splenic, inferior, and superior mesenteric capillaries and drain into the portal vein from the visceral peritoneum. However, the lymphatic system absorbs big molecules (MW > 5000), proteins, blood, and immune cells. Finally, both small and large molecules enter the systemic circulation [103]. Previous studies indicate that plasma proteins given intraperitoneally are dispersed throughout the body, similarly to plasma proteins given intravenously, and they are absorbed into systemic circulation [104]. We found and quantified labeled FN in plasma using a fluoroimager and a fluorometer, indicating that labeled pFN enters plasma from the intraperitoneal space and remains intact as a protein. In addition, compared to intravenous injection, a larger volume of solution can be

administered intraperitoneally [105]. Therefore, in our experiment, the intraperitoneal route of solution administration is an appropriate method for labeled FN injection. Studies have shown that pFN accumulates in several tissues (liver, brain, testis, heart, lungs, and bone) [53, 106], and the result of our study shows that pFN can also highly accumulate in adipose tissue. In 1981, Oh et al. used human pFN for injection into mice; human IgG injection was employed for the control group. The human FN concentration in the plasma samples was measured using a radioimmunoassay. Indirect immunofluorescence was utilized for observing pFN in the tissues. By using indirect immunofluorescent staining and species-specific antisera, pFN was localized in tissue sections from pFN-injected and control mice. Antihuman FN stained the tissues of mice receiving human FN injections but not the tissues of mice not receiving injections. Also, they gave the mice an injection of radiolabeled FN and saw an accumulation of radioactivity in the tissues that was higher than in the plasma and came to the conclusion that pFN could be incorporated into the tissues [107]. In 2007, Moretti et al. calculated the fraction of pFN to total FN in each tissue in their experiment by comparing the amount of FN in the tissue of wild-type mice and knock-in mice having constitutive inclusion of the EDA exon of the FN gene ($EDA^{+/+}$strain). The quantity of pFN in the plasma of the $EDA^{+/+}$strain has significantly decreased, although some plasma FN is still present. This suggested that EDA domain inhibits secretion of FN from hepatocytes. They showed that plasma is the source of a significant amount of the FN found in tissues' ECM. Western blot analysis was used in their work to measure the FN levels. The levels of EDA^{+}FN in tissues did not change between the $EDA^{WT/WT}$ and $EDA^{+/+}$CRE samples, indicating that the observed variations in tissue FN between the different genotypes were due to the incorporation of EDA^{-} FN from plasma into the ECM of tissues. They used 3E2 antiEDA monoclonal antibody to detect cellular FN having EDA domain [106]. Since the structure of plasma and cellular FN are the same and pFN just has an extra EDA domain, there is no antibody that can specifically detect pFN.

Some other studies also tried to visualize pFN in specific tissue with histology by injecting labeled pFN [35, 53, 108] . However, histology is not a precise method for measuring and quantifying pFN. This is rooted in the fact that there is not any accurate route for

measuring signals in microscopy, and moreover, in histology, we can just visualize a very limited and thin layer of tissue.

On the contrary, in fluorometry for each tissue, 10 mg of each tissue was analyzed, and the results were more precise when a larger volume of tissue was evaluated. There are other studies regarding the level of pFN in plasma in different diseases. In these studies, the level of pFN in plasma was calculated with ELISA or nephelometric immunoassays [97-101](the only form of FN seen in plasma is pFN.) In 2017, our laboratory (Mousa et al.) used the labeled pFN and the fluorometer to show the presence of pFN in the bone marrow vs bone tissue [109] and demonstrated that transglutaminase activity regulates pFN integration to bone. In our work, we improved these techniques and looked for new approaches to measure and map plasma FN. We observed the distribution of pFN throughout the body in our experiment. We gathered fluorometer data and signals from all tissues. Nearly all tissues had significantly stronger fluorescence signals in the pFN-injected group than in the control group. This shows that labeled pFN enters several tissues some of which have not reported before. The fluorometry result showed the accumulation of pFN in the liver, visceral adipose tissue, subcutaneous adipose tissue, and bone marrow. All of these tissues play an important role in glucose metabolism. FN matrix assembly is significantly increased in elevated glucose levels because integrin activity is stimulated at high glucose levels [110]. There are limited studies regarding the role of pFN in adipogenesis. By interacting with Pref-1, FN can modulate adipogenesis and prevent adipocyte differentiation. Pref-1 is a factor that prevents adipocyte differentiation by activating ERK/MAPK (extracellular signal-regulated kinase/mitogen-activated protein kinase) [111]. By increasing pFN assembly from plasma into the preadipocyte extracellular matrix, FXIII-A functioned as a negative adipogenesis regulator [72]. pFN regulates 3T3-L1 cell adipogenesis, impacts insulin signaling, and controls cell proliferation and differentiation [72]. In mouse embryonic fibroblasts lacking FXIII-A, lipid accumulation increases, and pFN assembly into ECM decreases [72]. Furthermore, obesity affects the expression of FN in the VAT and SAT, and in obese people, FN expression is much lower and adversely correlated with body mass index [112].

For visualizing pFN, it is labeled with Alexa Fluor 680, which is a near-infrared (NIR) probe. High photon penetration, low light scattering, and little autofluorescence from living

tissues are benefits of NIR fluorescent probes, which make them useful for noninvasive molecular event mapping, determining the effectiveness of treatments, and tracking the disease progression in animal models [113]. For visualizing pFN under confocal microscopy, the tissues were prepared with frozen and paraffin embedding approaches. When the histological approaches were compared, cryosectioning appeared to be superior, with a significant difference between labeled and control specimens. Most researchers believe that the quenching of fluorescence is caused by the application of chemical fixing agents and high temperatures during the paraffin embedding procedure [114, 115]. Sectioning fat tissue using the frozen embedding approach is challenging because fat does not become hard enough to cut properly at temperatures ideal for cutting most other tissues, and we could not get a complete section from VAT and SAT. Zhanmu et al. suggested tertiary butanol (TBA) dehydrating paraffin embedding technique for maintenance of fluorescence during the paraffin embedding approach [96]. We use both traditional and TBA paraffin embedding techniques in our experiment. Contrary to cell culture, the FN fibrillar network cannot be observed in tissue with confocal microscopy. However, the intensity of the gray value is different between the control and pFN-treated groups [35, 53, 108]. According to fluorometer data, we expected the highest amount of labeled pFN in liver slides, and histology results support this expectation (the highest difference between the two groups was seen in liver slides prepared with the cryosectioning approach. Although the grey value intensity in all labeled pFN groups was higher than in control groups, the fluorescence signal was relatively weak and required further optimization.

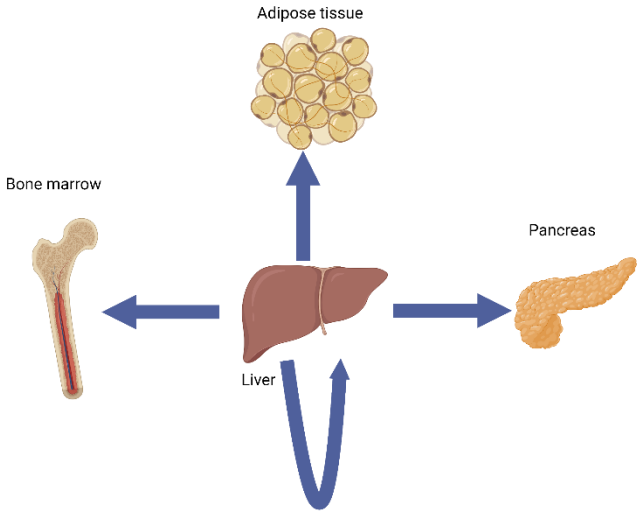

Figure 17. Distribution of pFN in metabolic tissues. pFN is generated by the liver, drains to plasma, and then goes to adipose tissue, pancreas, bone marrow, and liver.

6. Conclusions

According to our findings, fluorometry is a highly suitable way for measuring pFN matrix formation in different tissues. This study identified adipose tissue as tissues where pFN forms ECM and where it may have a novel role in regulating adipose tissue function.

7. Future directions

More experiments are needed to confirm our observations. The experiments can be done in future are listed below:

1- Quantification of labeled pFN in pFN knockout mouse models: In this study, we measured distribution of an extra amount of pFN in wild-type mice. In subsequent studies, measurements can be carried out in pFN knockout mice models, and the results can be compared to those from the present study.

2- The distribution of labeled pFN can be measured in the obese mouse. In the present study, adipose tissue contained a significant amount of labeled pFN. In subsequent studies, this technique can be used to measure the concentration of pFN in obese mouse adipose tissue and compare the results to those from the current study.

3- In Vivo Fluorescence Imaging can be used as one of the methods to evaluate distribution of pFN in the mouse body.

4- This method can be used in a wide range of knock-out mouse models to evaluate the effect of different pathological conditions on the distribution of pFN in the body and its accumulation in each tissue.

REFERENCES

1. Hall, J.E. and M.E. Hall, *Guyton and Hall textbook of medical physiology e-Book*. 2020: Elsevier Health Sciences.
2. Abdel-Misih, S.R. and M. Bloomston, *Liver anatomy.* Surgical Clinics, 2010. **90**(4): p. 643-653.
3. Meex, R.C. and M.J. Watt, *Hepatokines: linking nonalcoholic fatty liver disease and insulin resistance.* Nature Reviews Endocrinology, 2017. **13**(9): p. 509-520.
4. Lai, K.K., D. Kolippakkam, and L. Beretta, *Comprehensive and quantitative proteome profiling of the mouse liver and plasma.* Hepatology, 2008. **47**(3): p. 1043-1051.
5. Nicholson, J., M. Wolmarans, and G. Park, *The role of albumin in critical illness.* British journal of anaesthesia, 2000. **85**(4): p. 599-610.
6. De Feo, P., F.F. Horber, and M.W. Haymond, *Meal stimulation of albumin synthesis: a significant contributor to whole body protein synthesis in humans.* American Journal of Physiology-Endocrinology And Metabolism, 1992. **263**(4): p. E794-E799.
7. Fleck, A., et al., *Increased vascular permeability: a major cause of hypoalbuminaemia in disease and injury.* The Lancet, 1985. **325**(8432): p. 781-784.
8. Aziz-Seible, R.S. and C.A. Casey, *Fibronectin: functional character and role in alcoholic liver disease.* World journal of gastroenterology: WJG, 2011. **17**(20): p. 2482.
9. Schwarzbauer, J.E., *Fibronectin: from gene to protein.* Current opinion in cell biology, 1991. **3**(5): p. 786-791.
10. Hynes, R.O., *Structure of fibronectins*, in *Fibronectins*. 1990, Springer. p. 113-175.
11. Tamkun, J. and R. Hynes, *Plasma fibronectin is synthesized and secreted by hepatocytes.* Journal of Biological Chemistry, 1983. **258**(7): p. 4641-4647.
12. Zardi, L., et al., *Concentration of fibronectin in plasma of tumor-bearing mice and synthesis by Ehrlich ascites tumor cells.* Cancer research, 1979. **39**(9): p. 3774-3779.
13. Paul, J., et al., *Cell-type-specific fibronectin subunits generated by alternative splicing.* Journal of Biological Chemistry, 1986. **261**(26): p. 12258-12265.
14. Schwarzbauer, J.E., *Alternative splicing of fibronectin: three variants, three functions.* Bioessays, 1991. **13**(10): p. 527-533.
15. To, W.S. and K.S. Midwood, *Plasma and cellular fibronectin: distinct and independent functions during tissue repair.* Fibrogenesis & tissue repair, 2011. **4**(1): p. 1-17.
16. Ali, I.U., *Phosphorylation of fibronectin in quiescent and growing cell cultures.* FEBS letters, 1983. **151**(1): p. 45-48.
17. George, E.L., et al., *Defects in mesoderm, neural tube and vascular development in mouse embryos lacking fibronectin.* Development, 1993. **119**(4): p. 1079-1091.
18. Hörmann, H. and M. Seidl, *Affinity chromatography on immobilized fibrin monomer, III. The fibrin affinity center of fibronectin.* Hoppe-Seyler's Zeitschrift fur physiologische Chemie, 1980. **361**(9): p. 1449-1452.
19. Singh, P., C. Carraher, and J.E. Schwarzbauer, *Assembly of fibronectin extracellular matrix.* Annual review of cell and developmental biology, 2010. **26**: p. 397-419.
20. !!! INVALID CITATION !!! {}.
21. Aota, S.-i., M. Nomizu, and K.M. Yamada, *The short amino acid sequence Pro-His-Ser-Arg-Asn in human fibronectin enhances cell-adhesive function.* Journal of Biological Chemistry, 1994. **269**(40): p. 24756-24761.

22. Fogerty, F.J., et al., *Inhibition of binding of fibronectin to matrix assembly sites by anti-integrin (alpha 5 beta 1) antibodies.* The Journal of cell biology, 1990. **111**(2): p. 699-708.
23. Hynes, R.O., *Interactions of fibronectins*, in *Fibronectins*. 1990, Springer. p. 84-112.
24. Sottile, J. and D.C. Hocking, *Fibronectin polymerization regulates the composition and stability of extracellular matrix fibrils and cell-matrix adhesions.* Molecular biology of the cell, 2002. **13**(10): p. 3546-3559.
25. Engler, A.J., et al., *A novel mode of cell detachment from fibrillar fibronectin matrix under shear.* Journal of cell science, 2009. **122**(10): p. 1647-1653.
26. Kurkinen, M., et al., *Sequential appearance of fibronectin and collagen in experimental granulation tissue.* Laboratory Investigation; a Journal of Technical Methods and Pathology, 1980. **43**(1): p. 47-51.
27. Kubow, K.E., et al., *Mechanical forces regulate the interactions of fibronectin and collagen I in extracellular matrix.* Nature communications, 2015. **6**(1): p. 1-11.
28. Grinnell, F., R.E. Billingham, and L. Burgess, *Distribution of fibronectin during wound healing in vivo.* Journal of Investigative Dermatology, 1981. **76**(3): p. 181-189.
29. Mao, Y. and J.E. Schwarzbauer, *Stimulatory effects of a three-dimensional microenvironment on cell-mediated fibronectin fibrillogenesis.* Journal of cell science, 2005. **118**(19): p. 4427-4436.
30. Saba, T.M. and E. Jaffe, *Plasma fibronectin (opsonic glycoprotein): its synthesis by vascular endothelial cells and role in cardiopulmonary integrity after trauma as related to reticuloendothelial function.* The American journal of medicine, 1980. **68**(4): p. 577-594.
31. Trial, J., et al., *Inflammation and ischemia: macrophages activated by fibronectin fragments enhance the survival of injured cardiac myocytes.* Experimental Biology and Medicine, 2004. **229**(6): p. 538-545.
32. Patten, J. and K. Wang, *Fibronectin in development and wound healing.* Advanced Drug Delivery Reviews, 2021. **170**: p. 353-368.
33. Ni, H., et al., *Plasma fibronectin promotes thrombus growth and stability in injured arterioles.* Proceedings of the National Academy of Sciences, 2003. **100**(5): p. 2415-2419.
34. Matuskova, J., et al., *Decreased plasma fibronectin leads to delayed thrombus growth in injured arterioles.* Arteriosclerosis, thrombosis, and vascular biology, 2006. **26**(6): p. 1391-1396.
35. Kumra, H., et al., *Roles of fibronectin isoforms in neonatal vascular development and matrix integrity.* PLoS biology, 2018. **16**(7): p. e2004812.
36. Owens, M.R. and C.D. Cimino, *Synthesis of fibronectin by the isolated perfused rat liver.* 1982.
37. Liu, X.Y., et al., *Fibronectin expression is critical for liver fibrogenesis in vivo and in vitro.* Molecular Medicine Reports, 2016. **14**(4): p. 3669-3675.
38. Manabe, R.-i., N. Oh-e, and K. Sekiguchi, *Alternatively spliced EDA segment regulates fibronectin-dependent cell cycle progression and mitogenic signal transduction.* Journal of Biological Chemistry, 1999. **274**(9): p. 5919-5924.
39. Altrock, E., et al., *Inhibition of fibronectin deposition improves experimental liver fibrosis.* Journal of hepatology, 2015. **62**(3): p. 625-633.
40. Erturk, A., et al., *Serum fibronectin levels in acute and chronic viral hepatitis patients.* The Malaysian Journal of Medical Sciences: MJMS, 2014. **21**(1): p. 29.
41. Vassilopoulos, D. and L.H. Calabrese, *Management of rheumatic disease with comorbid HBV or HCV infection.* Nature Reviews Rheumatology, 2012. **8**(6): p. 348-357.
42. Lucena, S., A.P. CL, and B. Guerrero, *Fibronectin. Structure and functions associated to hemostasis. Review.* Investigacion Clinica, 2007. **48**(2): p. 249-262.
43. Kandemir, O., et al., *Fibronectin levels in chronic viral hepatitis and response of this protein to interferon therapy.* Hepato-gastroenterology, 2004. **51**(57): p. 811-814.

44. Chen, Y., et al., *Fibronectin predicts the outcome of acute-on-chronic hepatitis B liver failure.* International Health, 2015. **7**(1): p. 67-72.
45. El-Serag, H.B., *Epidemiology of hepatocellular carcinoma.* Clinics in liver disease, 2001. **5**(1): p. 87-107.
46. Kim, H., et al., *Serum fibronectin distinguishes the early stages of hepatocellular carcinoma.* Scientific reports, 2017. **7**(1): p. 1-9.
47. Moriya, K., et al., *Fibronectin is essential for survival but is dispensable for proliferation of hepatocytes in acute liver injury in mice.* Hepatology, 2012. **56**(1): p. 311-321.
48. Caputi, M., C. Melo, and F. Baralle, *Regulation of fibronectin expression in rat regenerating liver.* Nucleic acids research, 1995. **23**(2): p. 238-243.
49. Sawada, N., et al., *Extracellular matrix components influence DNA synthesis of rat hepatocytes in primary culture.* Experimental cell research, 1986. **167**(2): p. 458-470.
50. Jiang, X., et al., *Method development of efficient protein extraction in bone tissue for proteome analysis.* Journal of proteome research, 2007. **6**(6): p. 2287-2294.
51. Salmon, C.R., et al., *Proteomic analysis of human dental cementum and alveolar bone.* Journal of proteomics, 2013. **91**: p. 544-555.
52. Velling, T., et al., *Polymerization of type I and III collagens is dependent on fibronectin and enhanced by integrins α11β1and α2β1.* Journal of Biological Chemistry, 2002. **277**(40): p. 37377-37381.
53. Bentmann, A., et al., *Circulating fibronectin affects bone matrix, whereas osteoblast fibronectin modulates osteoblast function.* Journal of Bone and Mineral Research, 2010. **25**(4): p. 706-715.
54. Stein, G.S. and J.B. Lian, *Molecular mechanisms mediating proliferation/differentiation interrelationships during progressive development of the osteoblast phenotype.* Endocrine reviews, 1993. **14**(4): p. 424-442.
55. Moursi, A.M., et al., *Fibronectin regulates calvarial osteoblast differentiation.* Journal of cell science, 1996. **109**(6): p. 1369-1380.
56. Grzesik, W.J. and P.G. Robey, *Bone matrix RGD glycoproteins: immunolocalization and interaction with human primary osteoblastic bone cells in vitro.* Journal of Bone and Mineral Research, 1994. **9**(4): p. 487-496.
57. Moursi, A.M., R.K. Globus, and C.H. Damsky, *Interactions between integrin receptors and fibronectin are required for calvarial osteoblast differentiation in vitro.* Journal of cell science, 1997. **110**(18): p. 2187-2196.
58. Gramoun, A., et al., *Fibronectin inhibits osteoclastogenesis while enhancing osteoclast activity via nitric oxide and interleukin-1β-mediated signaling pathways.* Journal of cellular biochemistry, 2010. **111**(4): p. 1020-1034.
59. Lopatin, D.E., et al., *Concentrations of fibronectin in the sera and crevicular fluid in various stages of periodontal disease.* Journal of Clinical Periodontology, 1989. **16**(6): p. 359-364.
60. TALONPOIKA, J., et al., *Gingival crevicular fluid fibronectin degradation in periodontal health and disease.* European Journal of Oral Sciences, 1989. **97**(5): p. 415-421.
61. Kapila, Y.L., H. Lancero, and P.W. Johnson, *The response of periodontal ligament cells to fibronectin.* Journal of periodontology, 1998. **69**(9): p. 1008-1019.
62. Huynh, Q.N., et al., *Specific fibronectin fragments as markers of periodontal disease status.* Journal of periodontology, 2002. **73**(10): p. 1101-1110.
63. Larjava, H., et al., *Fibronectin fragmentation induced by dental plaque and Bacteroides gingivalis.* European Journal of Oral Sciences, 1987. **95**(4): p. 308-314.
64. Thesleff, I., et al., *Changes in the matrix proteins, fibronectin and collagen, during differentiation of mouse tooth germ.* Developmental Biology, 1979. **70**(1): p. 116-126.

65. Saito, K., et al., *Interaction between fibronectin and β1 integrin is essential for tooth development.* PLoS One, 2015. **10**(4): p. e0121667.
66. Sawada, T. and A. Nanci, *Spatial distribution of enamel proteins and fibronectin at early stages of rat incisor tooth formation.* Archives of oral biology, 1995. **40**(11): p. 1029-1038.
67. Mizuno, M. and Y. Banzai, *Calcium ion release from calcium hydroxide stimulated fibronectin gene expression in dental pulp cells and the differentiation of dental pulp cells to mineralized tissue forming cells by fibronectin.* International Endodontic Journal, 2008. **41**(11): p. 933-938.
68. Tang, J. and T. Saito, *Human plasma fibronectin promotes proliferation and differentiation of odontoblast.* Journal of Applied Oral Science, 2017. **25**: p. 299-309.
69. Zhang, X., et al., *Distribution of undulin, tenascin, and fibronectin in the human periodontal ligament and cementum: comparative immunoelectron microscopy with ultra-thin cryosections.* Journal of Histochemistry & Cytochemistry, 1993. **41**(2): p. 245-251.
70. Komboli, M.G., G.J. Kodovazenitis, and T.A. Katsorhis, *Comparative immunohistochemical study of the distribution of fibronectin in healthy and diseased root surfaces.* Journal of periodontology, 2009. **80**(5): p. 824-832.
71. Martinez, E. and V. Araujo, *In vitro immunoexpression of extracellular matrix proteins in dental pulpal and gingival human fibroblasts.* International Endodontic Journal, 2004. **37**(11): p. 749-755.
72. Myneni, V.D., K. Hitomi, and M.T. Kaartinen, *Factor XIII-A transglutaminase acts as a switch between preadipocyte proliferation and differentiation.* Blood, The Journal of the American Society of Hematology, 2014. **124**(8): p. 1344-1353.
73. Ariëns, R.A., et al., *The factor XIII V34L polymorphism accelerates thrombin activation of factor XIII and affects cross-linked fibrin structure.* Blood, The Journal of the American Society of Hematology, 2000. **96**(3): p. 988-995.
74. Örem, C., et al., *Plasma fibronectin level and its association with coronary artery disease and carotid intima-media thickness.* Coronary artery disease, 2003. **14**(3): p. 219-224.
75. Poon, M.-C., et al., *Hemopoietic origin of factor XIII A subunits in platelets, monocytes, and plasma. Evidence from bone marrow transplantation studies.* The Journal of clinical investigation, 1989. **84**(3): p. 787-792.
76. Wölpl, A., et al., *Coagulation factor XIII A and B subunits in bone marrow and liver transplantation.* Transplantation, 1987. **43**(1): p. 151-153.
77. Muszbek, L., et al., *Factor XIII: a coagulation factor with multiple plasmatic and cellular functions.* Physiological reviews, 2011. **91**(3): p. 931-972.
78. Barry, E. and D.F. Mosher, *Factor XIII cross-linking of fibronectin at cellular matrix assembly sites.* Journal of Biological Chemistry, 1988. **263**(21): p. 10464-10469.
79. Al-Jallad, H.F., et al., *Transglutaminase activity regulates osteoblast differentiation and matrix mineralization in MC3T3-E1 osteoblast cultures.* Matrix biology, 2006. **25**(3): p. 135-148.
80. Nurminskaya, M. and M.T. Kaartinen, *Transglutaminases in mineralized tissues.* Front Biosci, 2006. **11**(2): p. 1591-1606.
81. Nakano, Y., et al., *Expression and localization of plasma transglutaminase factor XIIIA in bone.* Journal of Histochemistry & Cytochemistry, 2007. **55**(7): p. 675-685.
82. Cui, C., et al., *Transglutaminase activity arising from Factor XIIIA is required for stabilization and conversion of plasma fibronectin into matrix in osteoblast cultures.* Bone, 2014. **59**: p. 127-138.
83. Cui, C. and M.T. Kaartinen, *Serotonin (5-HT) inhibits Factor XIII-A-mediated plasma fibronectin matrix assembly and crosslinking in osteoblast cultures via direct competition with transamidation.* Bone, 2015. **72**: p. 43-52.
84. Karsenty, G. and V. K. Yadav, *Regulation of bone mass by serotonin: molecular biology and therapeutic implications.* Annual review of medicine, 2011. **62**: p. 323-331.

85. Ducy, P. and G. Karsenty, *The two faces of serotonin in bone biology.* Journal of Cell Biology, 2010. **191**(1): p. 7-13.
86. Yadav, V.K., et al., *Lrp5 controls bone formation by inhibiting serotonin synthesis in the duodenum.* Cell, 2008. **135**(5): p. 825-837.
87. Al Shoyaib, A., S.R. Archie, and V.T. Karamyan, *Intraperitoneal route of drug administration: should it be used in experimental animal studies?* Pharmaceutical research, 2020. **37**(1): p. 1-17.
88. Morton, D., et al., *Refining procedures for the administration of substances.* Laboratory animals, 2001. **35**(1): p. 1-41.
89. Aune, S., *Transperitoneal exchange: IV. The effect of transperitoneal fluid transport on the transfer of solutes.* Scandinavian Journal of Gastroenterology, 1970. **5**(4): p. 241-252.
90. Hartveit, F. and S. Thunold, *Peritoneal fluid volume and the oestrus cycle in mice.* Nature, 1966. **210**(5041): p. 1123-1125.
91. Aune, S., *Transperitoneal exchange: II. Peritoneal blood flow estimated by hydrogen gas clearance.* Scandinavian Journal of Gastroenterology, 1970. **5**(2): p. 99-104.
92. Kuzlan, M., et al., *Peritoneal surface area and its permeability in rats.* Peritoneal dialysis international, 1997. **17**(3): p. 295-300.
93. Fedorko, M.E., J. Hirsch, and B. Fried, *Studies on transport of macromolecules and small particles across mesothelial cells of the mouse omentum: II. Kinetic features and metabolic requirements.* Experimental cell research, 1971. **69**(2): p. 313-323.
94. Christie, R.M., *Fluorescent dyes.* Handbook of textile and industrial dyeing, 2011: p. 562-587.
95. Kawelke, N., et al., *Isoform of fibronectin mediates bone loss in patients with primary biliary cirrhosis by suppressing bone formation.* Journal of Bone and Mineral Research, 2008. **23**(8): p. 1278-1286.
96. Zhanmu, O., et al., *Maintenance of fluorescence during paraffin embedding of fluorescent protein-labeled specimens.* Frontiers in neuroscience, 2019. **13**: p. 752.
97. Zerlauth, G. and G. Wolf, *Plasma fibronectin as a marker for cancer and other diseases.* The American journal of medicine, 1984. **77**(4): p. 685-689.
98. Mosher, D.F., *Fibronectin and liver disease.* Hepatology, 1986. **6**(6): p. 1419-1421.
99. Gluud, C., A. Dejgaard, and I. Clemmensen, *Plasma fibronectin concentrations in patients with liver diseases.* Scandinavian Journal of Clinical and Laboratory Investigation, 1983. **43**(6): p. 533-537.
100. Gabrielli, G.B., et al., *Plasma fibronectin in liver cirrhosis and its diagnostic value.* Clinica chimica acta, 1986. **160**(3): p. 289-296.
101. Labat-Robert, J. and L. Robert, *Modifications of fibronectin in age-related diseases: diabetes and cancer.* Archives of gerontology and geriatrics, 1984. **3**(1): p. 1-10.
102. Zhang, Y., et al., *Association study between fibronectin and coronary heart disease.* Clinical Chemistry and Laboratory Medicine (CCLM), 2006. **44**(1): p. 37-42.
103. Flessner, M., R. Dedrick, and J. Schultz, *Exchange of macromolecules between peritoneal cavity and plasma.* American Journal of Physiology-Heart and Circulatory Physiology, 1985. **248**(1): p. H15-H25.
104. Regoeczi, E., et al., *Absorption of plasma proteins from peritoneal cavity of normal rats.* American Journal of Physiology-Endocrinology and Metabolism, 1989. **256**(4): p. E447-E452.
105. Turner, P.V., et al., *Administration of substances to laboratory animals: routes of administration and factors to consider.* Journal of the American Association for Laboratory Animal Science, 2011. **50**(5): p. 600-613.
106. Moretti, F.A., et al., *A major fraction of fibronectin present in the extracellular matrix of tissues is plasma-derived.* Journal of Biological Chemistry, 2007. **282**(38): p. 28057-28062.

107. Oh, E., M. Pierschbacher, and E. Ruoslahti, *Deposition of plasma fibronectin in tissues.* Proceedings of the National Academy of Sciences, 1981. **78**(5): p. 3218-3221.
108. Klemis, V., et al., *Circulating fibronectin contributes to mesangial expansion in a murine model of type 1 diabetes.* Kidney international, 2017. **91**(6): p. 1374-1385.
109. Mousa, A., et al., *Transglutaminases factor XIII-A and TG2 regulate resorption, adipogenesis and plasma fibronectin homeostasis in bone and bone marrow.* Cell Death & Differentiation, 2017. **24**(5): p. 844-854.
110. Miller, C.G., et al., *Effects of high glucose on integrin activity and fibronectin matrix assembly by mesangial cells.* Molecular biology of the cell, 2014. **25**(16): p. 2342-2350.
111. Wang, Y., et al., *Pref-1 interacts with fibronectin to inhibit adipocyte differentiation.* Molecular and cellular biology, 2010. **30**(14): p. 3480-3492.
112. Lee, S.H., et al., *Fibronectin gene expression in human adipose tissue and its associations with obesity-related genes and metabolic parameters.* Obesity surgery, 2013. **23**(4): p. 554-560.
113. Quek, C.-H. and K.W. Leong, *Near-infrared fluorescent nanoprobes for in vivo optical imaging.* Nanomaterials, 2012. **2**(2): p. 92-112.
114. Smith, S.E., et al., *Fluorescence imaging preparation methods for tissue scaffolds implanted into a green fluorescent protein porcine model.* Transgenic research, 2015. **24**(5): p. 911-919.
115. Swenson, E.S., et al., *Limitations of green fluorescent protein as a cell lineage marker.* Stem Cells, 2007. **25**(10): p. 2593-2600.